Cell Reports

Article

Anterior-posterior gradient in the integrated processing of forelimb movement direction and distance in macaque parietal cortex

Graphical abstract

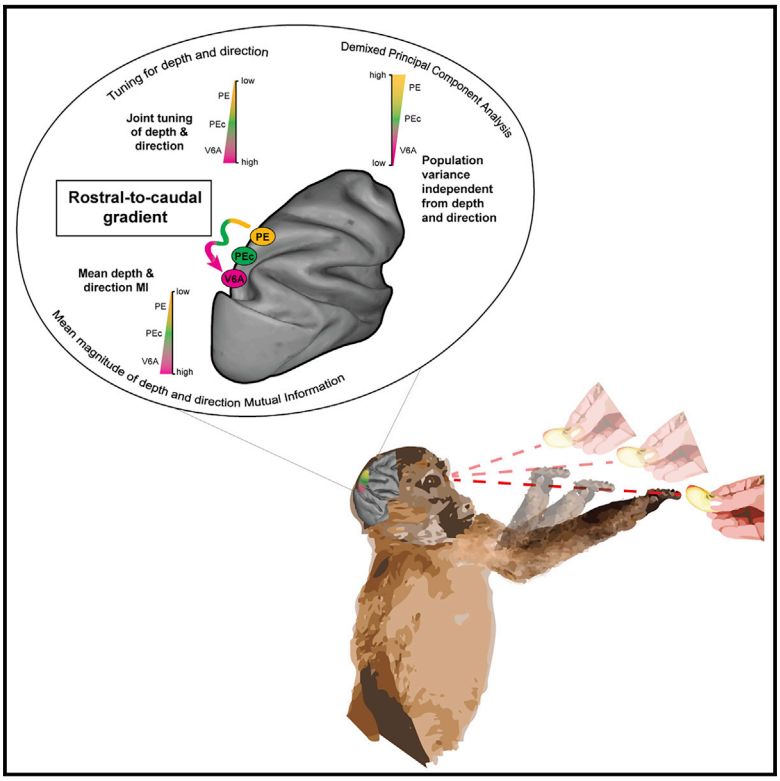

Highlights

- Parietal neurons show a mixture of responses during arm movements in 3D space
- Single-cell and population methods are used to tease apart movement-related signals
- Depth and directional signals converge along a rostrocaudal gradient
- Direction signals are strong in early phases, and depth is strong in perimovement epochs

Authors

Kostas Hadjidimitrakis, Marina De Vitis, Masoud Ghodrati, Matteo Filippini, Patrizia Fattori

Correspondence

kon.chatzidimitrakis@unibo.it (K.H.), patrizia.fattori@unibo.it (P.F.)

In brief

Hadjidimitrakis et al. investigate whether the direction and depth of arm movements are under independent control in the monkey parietal cortex during a 3D arm-movement task. Direction effects are stronger in early phases, whereas depth signals prevail during movement. Direction- and depth-related information converges along a rostrocaudal gradient.

Hadjidimitrakis et al., 2022, Cell Reports *41*, 111608
November 8, 2022
https://doi.org/10.1016/j.celrep.2022.111608

CellPress

Cell Reports

CellPress
OPEN ACCESS

Article

Anterior-posterior gradient in the integrated processing of forelimb movement direction and distance in macaque parietal cortex

Kostas Hadjidimitrakis,[1,3,4,*] Marina De Vitis,[1,3] Masoud Ghodrati,[2] Matteo Filippini,[1] and Patrizia Fattori[1,*]
[1]Department of Biomedical and Neuromotor Sciences, University of Bologna, Piazza di Porta San Donato 2, 40126 Bologna, Italy
[2]Department of Physiology and Biomedicine Discovery Institute, Monash University, Clayton, VIC 3800, Australia
[3]These authors contributed equally
[4]Lead contact
*Correspondence: kon.chatzidimitrakis@unibo.it (K.H.), patrizia.fattori@unibo.it (P.F.)
https://doi.org/10.1016/j.celrep.2022.111608

SUMMARY

A major issue in modern neuroscience is to understand how cell populations present multiple spatial and motor features during goal-directed movements. The direction and distance (depth) of arm movements often appear to be controlled independently during behavior, but it is unknown whether they share neural resources or not. Using information theory, singular value decomposition, and dimensionality reduction methods, we compare direction and depth effects and their convergence across three parietal areas during an arm movement task. All methods show a stronger direction effect during early movement preparation, whereas depth signals prevail during movement execution. Going from anterior to posterior sectors, we report an increased number of cells processing both signals and stronger depth effects. These findings suggest a serial direction and depth processing consistent with behavioral evidence and reveal a gradient of joint versus independent control of these features in parietal cortex that supports its role in sensorimotor transformations.

INTRODUCTION

An overarching aim of modern neuroscience is to understand how populations of cells across different parts of the nervous system interact in a dynamic manner, which allows the precise coordination of our perception and action. Like in other primates, a large proportion of what we do in our daily lives involves reaching with the arm and grasping objects located in the three-dimensional (3D) peripersonal space. Although every arm movement occurs in 3D space, it has become traditional among researchers to make a distinction between movement direction and amplitude or depth, i.e., how far the arm extends to reach its target. However, after over three decades of research, it is still under debate as to whether the brain specifies these two movement parameters independently. Numerous psychophysical and lesion studies suggest that reach coordinates are processed by separate neuronal channels (Soechting and Flanders, 1989; Gordon et al., 1994; Baylis and Baylis, 2001; Sainburg et al., 2003; Vindras et al., 2005; Bagesteiro et al., 2006; Van Pelt and Medendorp, 2008; Danckert et al., 2009; Tramper and Gielen, 2011; Apker and Buneo, 2012; Lefrançois and Messier, 2019). However, other psychophysical evidence is in line with common neural resources (Bhat and Sanes, 1998; Medendorp et al., 2003; Messier and Kalaska, 1999; Sarlegna and Blouin, 2010; Wijdenes et al., 2013). In comparison with the extensive psychophysical work, relatively few studies in primate premotor and motor cortex have addressed simultaneously the coding of movement distance and direction (Churchland et al., 2006; Even-Chen et al., 2017; Fu et al., 1993, 1995; Messier and Kalaska, 2000; Naselaris et al., 2006). In the parietal cortex, only a handful of studies have directly investigated the neural correlates of movement direction and depth during naturalistic arm movements in 3D space (Hadjidimitrakis et al., 2014a, 2015; Lacquaniti et al., 1995; De Vitis et al., 2019). These studies provided mixed results, supporting both joint and independent control; however, this could be attributed to different task contexts and idiosyncratic differences among animals and recording locations.

Contemporary research has established that the posterior parietal cortex (PPC) is involved in the processing of spatial information and in the control of goal-directed behavior (Andersen et al., 2014; Hadjidimitrakis et al., 2019; Husain and Nachev, 2007). Single neurons in the PPC process diverse types of motor information, for example, reach direction and hand grasping configuration (Chen et al., 2009; Lehmann and Scherberger, 2013; Michaels and Scherberger, 2018), and both spatial and temporal aspects of the same effector, like gaze position and speed (Diomedi et al., 2020), and some PPC cells encode both spatial and cognitive parameters, like decision-related signals and imagined movements (de Lafuente et al., 2015; Zhang et al., 2017). However, it remains unclear how this computational principle of mixed selectivity is implemented also in the control of reach parameters and how parietal populations integrate information about the

Cartesian axes of the 3D environment during arm reaching. One possibility is that reach direction and distance are encoded by distinct neural circuits and/or separate neuronal populations within the same cortical area, in line with the majority of the psychophysical studies. Interestingly, an early neurophysiological study provided strong support for this view, reporting that the spatial coordinates (azimuth, distance, and elevation) of reaching targets were encoded by distinct subpopulations in Brodmann's area 5 (area PE) in parietal cortex (Lacquaniti et al., 1995). Another possibility is that reach coordinates are encoded by the same population of neurons, but at distinct times during the planning and execution of the movement. This view fits with behavioral evidence suggesting a serial processing of movement direction and depth signals, with direction being specified first (Bhat and Sanes, 1998), and is supported by neurophysiological work in the premotor cortex, although with 2D reaches performed with a joystick (Churchland et al., 2006; Even-Chen et al., 2017; Fu et al., 1993, 1995; Messier and Kalaska, 2000). A third possibility, combining the first two scenarios, is that reach direction and depth are processed by overlapping populations of PPC cells and also show different temporal dynamics. In favor of this view, we provided some preliminary evidence from the caudal PPC (Hadjidimitrakis et al., 2014a, 2015).

Here, we tested these alternatives by analyzing neural discharges from single PPC neurons in the same monkey, while it gazed and reached toward targets located at different distances and directions. We recorded in two macaques from three different areas along the anteroposterior (AP) axis of the medial PPC, namely PE (anterior), the area caudal to it (area PEc), and the more posterior visual area V6A that are involved in reaching control (Bosco et al., 2010; Fattori et al., 2017; Ferraina et al., 2001, 2009; Hawkins et al., 2013; Lacquaniti et al., 1995; Marzocchi et al., 2008; McGuire and Sabes, 2011; Shi et al., 2013). Anatomical connectivity studies in macaques and neuroimaging work in humans suggest some degree of AP functional specialization, with anterior PPC sectors receiving predominantly proprioceptive input and being involved mostly in movement execution and posterior sectors relying more on visual input and controlling movement planning (Bakola et al., 2010, 2013; Barany et al., 2014; Filimon et al., 2009; Gamberini et al., 2009, 2018; Johnson et al., 1996). These anatomical and functional trends are also supported by recent accounts of PPC organization that reinstate a distinction between low- and high-level associative areas in line with the original assignment of posterior parietal fields to areas 5 and 7 of Brodmann (Gamberini et al., 2020). Given this evidence, in the present work we examined whether the various motor parameters are processed following different schemes across PPC subdivisions. We found that, in all areas, distance and direction information showed a partial anatomical segregation, with a clear trend of increasing convergence along the AP axis, i.e., going from PE to V6A. We also report a common pattern of temporal dynamics, with direction signals being stronger immediately after target fixation, whereas distance processing gradually increased and peaked around movement onset. Overall, our results suggest flexible spatial representations for reaching and further highlight the importance of anatomical and functional gradients in PPC.

RESULTS

Single-unit activity was recorded from the PPC in two monkeys while they performed an instructed-delay arm-reaching task (Figure 1A). During a trial, monkeys were first required to look at visual targets (light-emitting diodes, LEDs) for a variable delay period while keeping their arm still at a resting position (Figure 1A). When cued, (Figure 1A), they had to move their arm toward the target and hold it to receive a reward. The targets appeared in one of nine locations (3 depths × 3 directions), at eye level (Figure 1A). It should be mentioned that in our setup arm movements had an elevation component that could not be dissociated from movement distance because nearer targets were always associated with steeper elevation angles compared with farther ones (Figure 1A), so elevation could represent a potential confound in the distance effects. A total of 899 PPC neurons distributed across three neighboring areas in the PPC of two macaques (monkeys M1 and M2) were recorded (Figure 1B; V6A, 178 M1/153 M2; PEc, 184 M1/151 M2; PE, 87 M1/146 M2). The task epochs of interest were: (1) the early fixation epoch (FIX), from 50 to 450 ms after the monkey started to look at the LED target; (2) the preparation epoch (PLAN), the last 500 ms before the "go" cue; and (3) the reach epoch (REACH), from 200 ms before the arm movement onset until its end (Figure 1A; see also STAR Methods).

To investigate how neuronal activity of the entire recorded population evolved along the task progress, we computed the population activity in each area as the spike density function (SDF), averaging the discharges of all recorded cells for each of the nine task conditions. To appreciate the strength of modulations, Figure 1C shows the average population response for the task condition that evoked the strongest activity (Figure 1C, preferred) and the population response that evoked the weakest activity (Figure 1C nonpreferred), selected separately for each behavioral event of alignment (i.e., fixation onset and movement onset). In the preferred condition, the cumulative activity in each area started to increase before the arm movement onset and peaked just after it (Figure 1C, REACH). A modest inhibition of population activity was also observed during the fixation epoch in V6A (Figure 1C FIX) and in all three areas during the planning and execution of nonpreferred arm movements (Figure 1C, PLAN and REACH). The preferred and nonpreferred SDFs in all three areas started to diverge right before the fixation onset (Figure 1C, FIX) and this separation was maintained and became more evident during the course of the task. The strength of spatial selectivity measured as the difference in population activity between the preferred and the nonpreferred positions was high and statistically significant across all task epochs in V6A and PEc, while in PE it became statistically relevant when the movement planning was already ongoing (Figure 1C; permutation test, $p < 0.05$). The same trends were also evident in the individual population responses of the two monkeys (Figure S1).

Dynamic depth and direction tuning in the different task phases

We quantified the effects of depth and direction signals on the activity of single neurons. A two-way ANOVA ($p < 0.01$) revealed that target depth (near, intermediate, far, with respect to the body) and target direction (contralateral, center, ipsilateral,

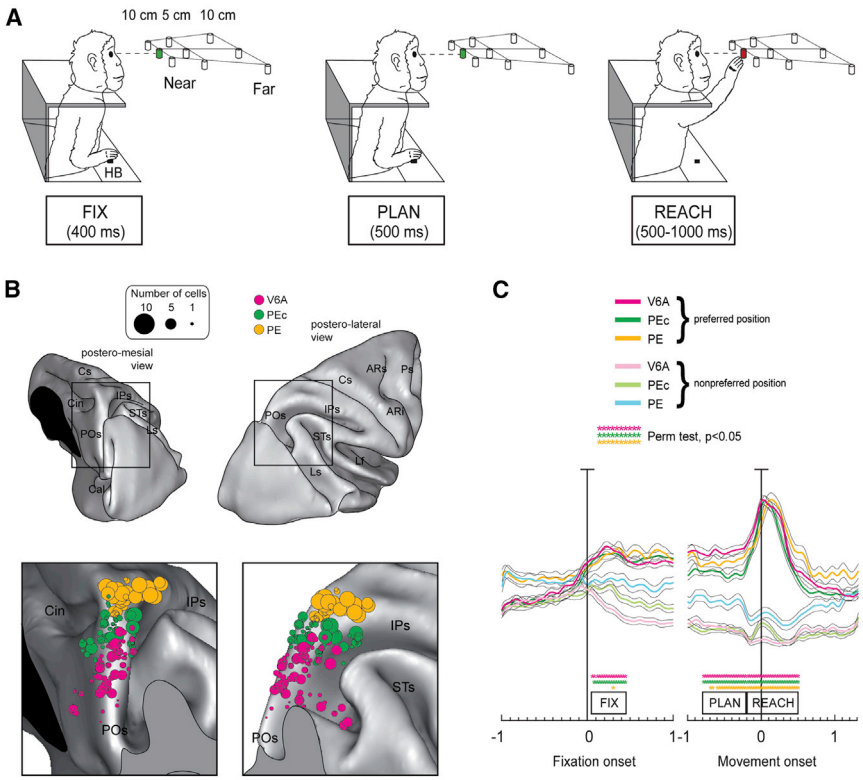

Figure 1. Behavioral task and recording sites

(A) Experimental setup and task sequence. Nine LEDs that were used as fixation and reaching targets were located at eye level. The distances of the three targets of the central row from mid-eye level are shown. HB, home button.

(B) Top: dorsomedial (left) and dorsolateral (right) view of a *Macaca fascicularis* right hemisphere reconstructed in 3D using Caret software (http://brainvis.wustl.edu/wiki/index.php/Caret:About). Bottom: magnified view of the dotted rectangles shown on top, showing the location and extent of recorded cells in V6A (pink), PEc (green), and PE (gold). ARs, arcuate sulcus superior ramus; ARi, arcuate sulcus inferior ramus; Cal, calcarine sulcus; Cin, cingulate sulcus; Cs, central sulcus; IPs, intraparietal sulcus; Lf, lateral fissure; Ls, lunate sulcus; POs, parieto-occipital sulcus; Ps, principal sulcus; STs, superior temporal sulcus.

(C) Average normalized SDF for the preferred (bright-colored curves) and nonpreferred positions (washed-out curves) of the recorded V6A, PEc, and PE populations (n = 331; n = 335; n = 233, respectively), aligned at the fixation and movement onset. Thin black lines in SDFs represent the standard error of the mean. Vertical bars in all SDF plots: 80% of normalized activity. Asterisks indicate statistical difference between the SDF curve in bins of 20 ms (permutation test, *p < 0.05).

with respect to the recording hemisphere) significantly influenced the firing rates of the majority of recorded neurons in the three areas (Figure 2A). Importantly, these modulations were differently distributed across the task epochs. All three areas showed a strong tuning of activity by direction information during the initial target fixation period (FIX), with a significantly higher fraction of cells specifically modulated by direction compared with the subsequent task epochs (Figure 2A; direction-only cells, two-proportion z test: FIX vs. PLAN p = 0.002/0.022/0.040 for V6A/PEc/PE, FIX vs. REACH p = 0.012/0.029/0.026). In contrast, in all areas, depth processing tended to increase during the task, and the proportion of cells with only depth tuning (Figure 2A, depth-only cells) was significantly higher during movement execution compared with early task stages (two-proportion z test: FIX vs. REACH p = 0.022/0.004/0.006 for V6A/PEc/PE).

In addition, the ANOVA revealed a third group of cells that were modulated by both depth and direction information (Figure 2A, "both"). Within each area, the fraction of cells tuned by both these factors increased only slightly along the task progress (V6A, 18%–22%; PEc, 11%–16%; PE, 2%–6%). Given the total incidence of depth and directional tuning in each epoch, we tested whether the proportions of cells tuned for both depth and direction were significantly higher from a chance rate and found that to be the case in almost all cases (two-sample binomial test, $p < 0.05$ in all area/epoch comparisons apart from FIX in PE). Interestingly, comparing joint directional and depth tuning across areas, we found a significantly higher proportion of cells tuned by both parameters in V6A with respect to the other two areas (two-sample binomial test, V6A vs. PEc, $p << 0.001$ in FIX and PLAN, p = 0.008 in REACH; V6A vs. PE, $p << 0.001$ in all epochs), and PEc had a significantly higher fraction than PE (two-sample binomial test, PEc vs. PE, $p << 0.001$ in all epochs). In sum, V6A, and to a lesser extent PEc, appeared as a site of convergence of depth and direction information.

Regarding the other two groups of cells with exclusive directional or depth tuning, PE had a significantly lower proportion with respect to PEc (two-sample binomial test, depth only, p = 0.0047 in FIX, $p < 0.001$ in PLAN, p = 0.036 in REACH; direction only, $p << 0.001$ in all epochs) and a highly significant lower proportion compared with V6A (two-sample binomial test, depth only, $p << 0.001$ in all epochs; direction only, $p << 0.001$ in all epochs). In contrast, comparing V6A with PEc revealed similar fractions of direction-specific tuning in all epochs (two-sample binomial test, direction only, $p > 0.05$), whereas the depth-specific modulations were more frequent in V6A during initial fixation and movement planning but not during movement execution (two-sample binomial test, depth only, p = 0.006/0.002 in FIX/PLAN, $p > 0.05$ in REACH). The main trends described above were also evident when looking separately at the results from each monkey (Table S1). To exclude a possible influence of variable movement time, due to different target depths, on neural modulation of activity quantified in epoch REACH, we also defined a movement epoch, hereafter called REACH_fixedTime, of a fixed duration of 300 ms, from movement onset until 300 ms after it. We performed a one-way ANOVA (factor depth) to quantify the proportion of cells modulated by depth in REACH_fixedTime within each area (V6A, 26%; PEc, 25%; PE, 21%) and compared the results with those obtained in the original

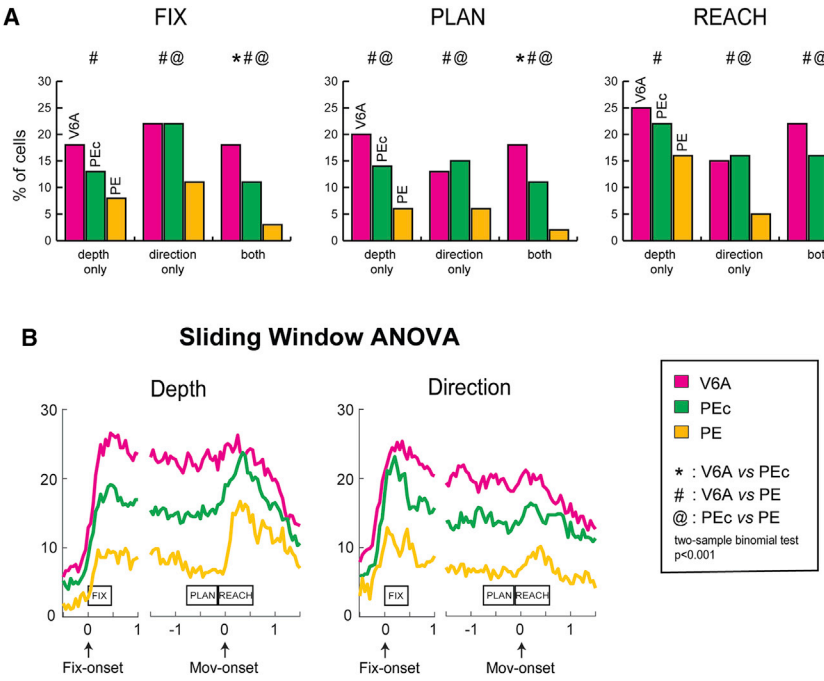

Figure 2. Population profile of depth and directional tuning

(A) Fraction of V6A (pink), PEc (green), and PE (gold) cells showing tuning for depth only, direction only, and both factors in the different task epochs (two-way ANOVA, $p < 0.01$).

(B) Percentage of tuned V6A (pink line), PEc (green line), and PE (gold line) cells by depth (left) and direction (right) in a sliding window (width, 200 ms; step, 50 ms) two-way ANOVA ($p < 0.01$). Trials are aligned at fixation and movement onset.

REACH epoch (V6A, 25%; PEc, 22%; PE, 16%). A two-proportion z test between results in REACH vs. REACH_fixedTime revealed no statistical difference for all comparisons ($p >> 0.05$).

To examine the evolution of tuning in finer temporal detail, we performed a sliding window ANOVA (Figure 2B; width, 200 ms; step, 50 ms). This analysis confirmed the different time courses of direction and depth effects across the three areas observed in the fixed-epochs analysis. The overall effect of depth was strong in V6A (~25%; Figure 2B, left) all along the task progress, i.e., from FIX to REACH, whereas in PEc and PE it was lower in FIX and PLAN and showed a marked increase in REACH (20% in PEc and 15% in PE; Figure 2B, left). Directionally tuned neurons had a similar trend in the three areas. Their incidence peaked during the early fixation epoch (FIX; 25% in V6A, 23% in PEc, 10% in PE; Figure 2B, right) and gradually decreased during the course of the trial.

In sum, at the level of single areas, the above analyses revealed a common trend of sequential direction and depth processing in line with earlier evidence from the premotor cortex (Messier and Kalaska, 2000; see also Ferraina et al., 2009, for depth processing). Importantly, at the network level, our results highlighted two additional trends: (1) a stronger influence of depth signals in the posterior PPC sector (V6A) and (2) a gradual transition from joint to independent coding of direction and depth information going from posterior to anterior PPC sites. In the subsequent sections, we performed several additional analyses to validate and deepen these findings.

Distinct temporal profile and anterior-posterior gradient in the strength and timing of directional and depth mutual information

We used information theory methods (Panzeri et al., 2007) and quantified the mutual information (MI) between the firing of the tuned cells and the depth or directional information. Since MI is a nonparametric measure of statistical dependency between two signals, it enabled a more direct quantification of a neuron's encoding strength of the two types of information. Furthermore, we examined binned neuronal data aligned at main task events, so we were able to compare the magnitude and temporal evolution of the MI between the three parietal areas. Figure 3 shows the mean depth and directional MI during two task intervals around fixation onset (Figure 3A) and movement onset (Figure 3B), across all tuned cells in the three areas (Figure 2). At each interval, MI was calculated with single-cell activity aligned at the corresponding task event. It should be mentioned that the trends of the mean MI results were consistent between the two monkeys (Figure S3), so the corresponding data were pooled together (Figure 3).

In the first interval around the fixation start (Figure 3A, vertical dashed line), there was a rapid increase of mean MI in all areas, with mean directional MI showing both an earlier peak time (~200 ms) and a higher peak amplitude compared with mean depth MI (Figure 3A). Overall, the highest peak values in both MI categories were observed in V6A (Figure 3A, pink line), with PEc and PE showing intermediate and low peak MI values, respectively (Figure 3A, green and gold lines). The difference in peak amplitude between directional and depth MI was larger in area PEc (Figure 3A, green lines). After about 0.5 s from the start of fixation, mean depth and direction MI in all areas dropped to levels that were halfway between baseline and peak values. Within each area, sustained levels of depth and direction MI were similar and, as for the peak MI magnitude, there was trend for MI to decrease, going from V6A to PE. Interestingly, peak MI levels for both direction and depth were reached later in PE with respect to V6A and PEc.

Around movement onset we observed in all areas higher depth MI values compared with the early fixation interval, whereas directional MI values were lower (Figure 3B). Directional MI peaked again slightly earlier compared with depth MI, but the amplitudes were 30%–50% smaller compared with depth MI peak amplitudes. Depth MI amplitude was doubled with respect to the sustained premovement levels in PE and PEc, and it increased by 30% in V6A, whereas the increase in direction MI was smaller (20%–25%) in all areas. Comparing the MI time

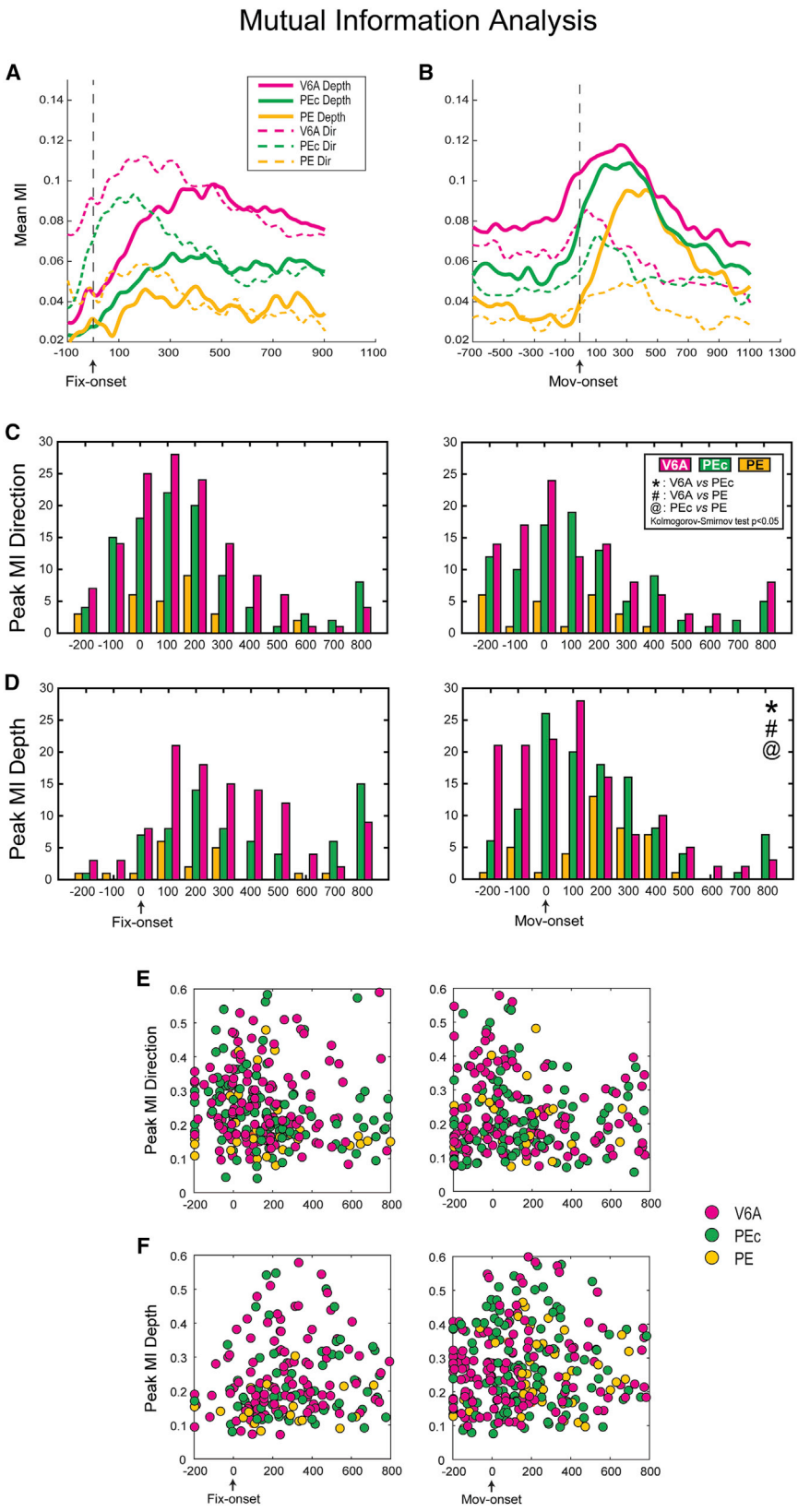

Figure 3. Population average depth and directional mutual information

(A–F) Mean magnitude of depth (solid lines) and directional (dashed lines) mutual information (MI) at fixation onset (A) and movement onset (B) across all tuned cells (two-way ANOVA, $p < 0.01$) in V6A, PEc, and PE. Distributions of time-to-peak MI estimated in single neurons of each area for direction (C) and depth (D) data and peak MI magnitude for direction (E) and depth (F) aligned at fixation onset (left) and movement onset (right).

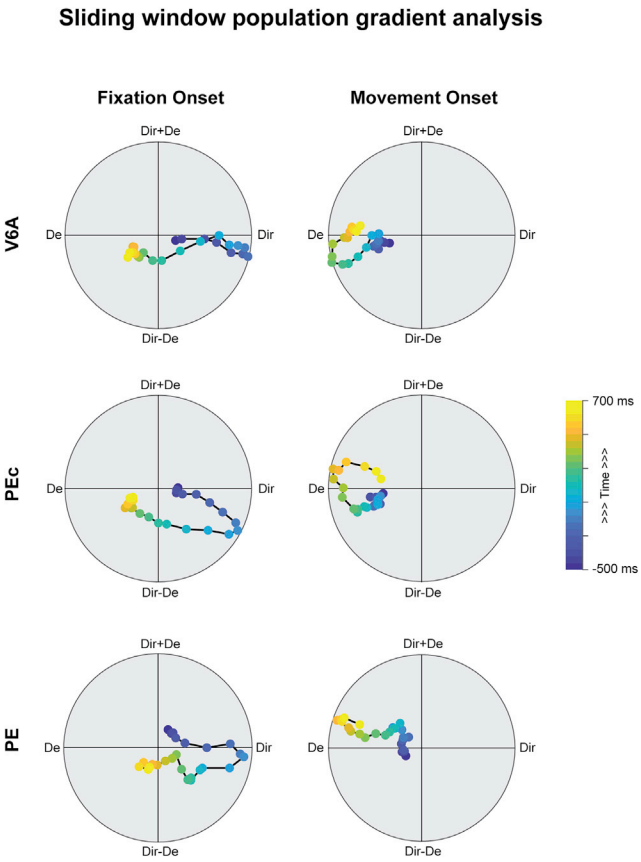

Figure 4. Evolution of depth and direction tuning in the population response

Sliding window population gradient analysis, showing the temporal evolution of depth and direction encoding in V6A, PEc, and PE. Each data point corresponds to the angle of the population's response field orientation, thus indicating which of the two variables has a stronger effect on activity at each time step. The distance from the center of the circle is proportional to the strength of tuning. Arrow lengths were averaged (vector summation) within each subpopulation and therefore they were not comparable across subpopulations. Plots are aligned at fixation onset (left) and movement onset (right).

course between the three areas (Figure 3B, vertical dashed line), at movement onset the depth MI was close to the peak value in V6A (Figure 3B, pink line), halfway between premovement level and peak value in PEc (Figure 3B, green line), and at the start of the increase in PE (Figure 3B, gold line). This trend was observed also in directional MI, although much less pronounced (Figure 3B, dashed lines). This difference in the depth MI time course between the three areas could reflect a serial processing of depth information during reach execution.

The time course of population MI was confirmed in the distributions of time-to-peak MI estimated in single neurons (Figures 3C and 3D). Comparing these distributions between the three areas at the fixation interval revealed no difference between them, for both direction and depth (Figures 3C and 3D, left; Kolmogorov-Smirnov test for V6A-PEc/V6A-PE/PEc-PE pairs: $p > 0.05$). Regarding the movement interval, for directional MI there was again no statistical difference in time-to-peak MI distributions between the areas (Figure 3C, right). In contrast, for depth MI (Figure 3D, right), all statistical comparisons between the three areas were significant (Kolmogorov-Smirnov test for V6A-PEc/V6A-PE/PEc-PE pairs: $p < 0.05$). This was in line with the significantly higher number of V6A neurons compared with the other two areas that showed peaks in depth MI before movement onset (two-sample binomial test: $p < 0.05$).

Similarly, there were significantly more V6A and PEc neurons with peaks in depth MI around movement onset (Figure 3D, right, 0 and 100 ms bins) compared with PE (binomial test: $p < 0.05$).

Apart from the time-to-peak MI distributions, we also examined the distributions of peak MI values between the three areas to directly compare the depth and direction effects (Figures 3E and 3F). At the fixation onset interval, directional peak MI was significantly higher in V6A compared with both PEc and PE (t test: $p < 0.05$). PE, in turn, had lower values of peak MI with respect to PEc (Figure 3E, left; t test: $p < 0.05$). Regarding depth, peak MI in PE cells was significantly lower than in both PEc and V6A (Figure 3F, left; t test: $p < 0.05$). For the time interval around movement onset, peak MI magnitudes for directional information were comparable between the three areas (Figure 3E, right; t test: $p > 0.05$), whereas depth peak MI in PE was significantly lower only in comparison with PEc (Figure 3F, right; t test: $p < 0.05$). In sum, this analysis at the single-cell level was in line with the population average MI findings and revealed a trend of higher peak MI values in more caudal sectors of the PPC.

Another important point regards the timing of peak directional and depth MI in single cells. As can be inferred from Figures 3C and 3D (left), at fixation interval peak directional MI occurred significantly earlier compared with depth MI in both PEc and V6A (Kolmogorov-Smirnov test: $p < 0.0001$), but not in PE (Kolmogorov-Smirnov test: $p > 0.05$). At the movement onset period (Figures 3C and 3D, right) the distributions of peak times for directional and depth MI were similar in PEc and V6A (Kolmogorov-Smirnov test: $p > 0.05$), whereas in PE, depth MI lagged behind directional MI (Kolmogorov-Smirnov test: $p < 0.05$). This analysis further confirmed, at the single-cell level, the earlier effect of direction compared with depth during the early fixation interval that was evident in the population MI (Figure 3A). This trend was also present in single neurons with both direction and depth effects (Figure S2).

Inseparable tuning by direction and depth in single cells and sequential processing of the two signals in the population response

To characterize the relationship between depth and direction in single neurons from the three areas in the same epochs of the ANOVA (i.e., in FIX, PLAN, and REACH), we performed gradient and singular value decomposition (SVD) analyses. In gradient analysis, neural responses for each neuron were organized into 3 × 3 (depth × direction) response matrices, where the firing rate is calculated for each pair of depth and direction positions and then a gradient field is computed (Figure S4). The resultant, or vector sum, of the gradient field summarizes which of the two variables has a larger influence on the firing rate of the cell (Buneo, 2011; Buneo and Andersen, 2012).

In the gradient analysis, we found that the proportion of cells tuned in at least one of the FIX, PLAN, or REACH epochs was 75% (N = 249/331) in V6A, 74% (N = 248/335) in PEc, and

Table 1. Separability analysis

	V6A (%, number)		PEc		PE	
	Separable	Inseparable	Separable	Inseparable	Separable	Inseparable
FIX only	2.8 (7/249)	19.6 (49/249)	1.6 (4/248)	14.1 (35/248)	1.9 (2/104)	18.2 (19/104)
PLAN only	2 (5/249)	5.6 (14/249)	0.8 (2/248)	14.9 (37/248)	1 (1/104)	9.6 (10/104)
REACH only	0.8 (2/249)	17.2 (43/249)	2 (5/248)	20.6 (51/248)	3.8 (4/104)	34.6 (36/104)
All	6.4 (16/249)	14.4 (36/249)	6 (16/248)	7.6 (19/248)	0 (0/104)	3.8 (4/104)

Incidence of separable and inseparable tuning in each task and epoch. "All" cells refer to cells that were tuned with gradient analysis in all the three epochs. "All" separable cells were found to be separable in at least one of the three epochs, whereas "all" inseparable cells were inseparable in all three epochs. Please note that the percentage values refer to the total number of cells tuned in an area in at least one epoch and that, for reasons of simplicity, the percentages of cells tuned in two epochs are not listed.

45% (n = 104/233) in PE. We then performed a sliding-window (300-ms window, 50-ms step; see also STAR Methods) population-level gradient analysis in these cells, to assess the temporal evolution of depth and direction encoding across the tuned responses in each area (Figure 4). Results from individual monkeys are shown in Figure S5. Each data point plots the angle of the population's response field orientation, thus indicating which of the two variables had a stronger effect on activity at each time step. The distance of each point from the center of the circle is proportional to the strength of tuning. After fixation onset (Figure 4, left), the population responses were very similar between the three areas, with direction effect being dominant. Around movement (Figure 4, right), the depth signals influenced much more strongly than direction the population responses in all areas. In sum, the population gradient analysis confirmed the dynamical processing of depth and direction signals observed with our previous analyses.

To examine the interaction between depth and direction effects at the single-cell level, we applied the SVD analysis in cells that were tuned in only one of these epochs and those that were tuned in all of them with the gradient analysis. SVD was applied in the tuned cells to define whether there is a gain-field relationship between the two variables that show a multiplicative and separable encoding, or whether the modulation of the neural response by one variable (e.g., depth) is affected by the other variable (e.g., direction), and thus the responses are inseparable (Bremner and Andersen, 2012; Pesaran et al., 2006). In other words, in separable cells the preference for a given depth (direction) does not change when direction (depth) is varied, whereas in inseparable ones it does change.

As shown in Table 1, in all three areas, the vast majority of cells with tuning present in only a single epoch were inseparable. In contrast, cells with sustained tuning across epochs showed an increased proportion of separable responses and were present mostly in PEc and V6A (PEc, 15/34; V6A, 16/52; Table 1, "All" cells). In sum, the combined gradient and SVD analysis in single cells revealed only small differences between the areas, regarding largely the group of cells with persistent tuning.

Separate components for direction and depth in the population activity

To further investigate how direction and depth signals are represented in the population activity, we applied a dimensionality reduction technique termed "demixed principal-component analysis" (dPCA) that is used to extract low-dimensional components of population activity that encode specific task parameters (Kobak et al., 2016).

To investigate whether there is an independent readout of depth and direction signals at the population response in the PPC, we computed the amount of variance that could be attributed to depth, direction, and interaction dPCA components. These components, together with the condition-independent component, represented the low-dimensional space of the population activity that was common to all three areas (Figure 5). As in our previous analyses, the population responses were aligned at the two main behavioral events, i.e., fixation and movement onset. Data from the two monkeys were pooled together since the results were consistent between them (Figure S6). Figure 5 shows that the condition-independent components accounted for the most of the neural variance (43%–77%) in all areas, in line with previous findings (Bosco et al., 2019; Michaels and Scherberger, 2018). Regarding the condition-independent variance, PE and V6A showed significantly different percentages (Figure 5, top and bottom, two-sample proportion binomial test: $p < 0.0001$). Within each of these two areas the condition-independent variance remained stable between the two activity alignments (two-sample proportion binomial test: $p > 0.05$). Interestingly, when population activity was aligned at fixation onset, the condition-independent variances were similar in PEc and V6A (45% vs. 43%, two-sample proportion binomial test: $p > 0.05$), whereas in population response aligned at movement onset, PEc variance was similar to that of PE (71% vs. 77%, two-sample proportion binomial test: $p > 0.05$). This large increase in the condition-independent variance in PEc during movement could reflect the fact that the task conditions are more similar in that phase (i.e., upward movements away from body) than during the initial fixation phase. Importantly, we found that in all areas the condition-dependent variance was explained mostly by separate depth-dependent and direction-dependent dPCA components that, within each area, were almost equal in the period after fixation onset (Figure 5, left).

Conversely, in the period around movement onset, the depth-dependent variance was 2–3 times—depending on the area—higher with respect to the direction-dependent variance (Figure 5, right). Interaction-dependent components accounted for a small percentage of variance in all three areas (1%–10%). For both alignments of the population response, the highest percentage of interaction-dependent variance was found in V6A

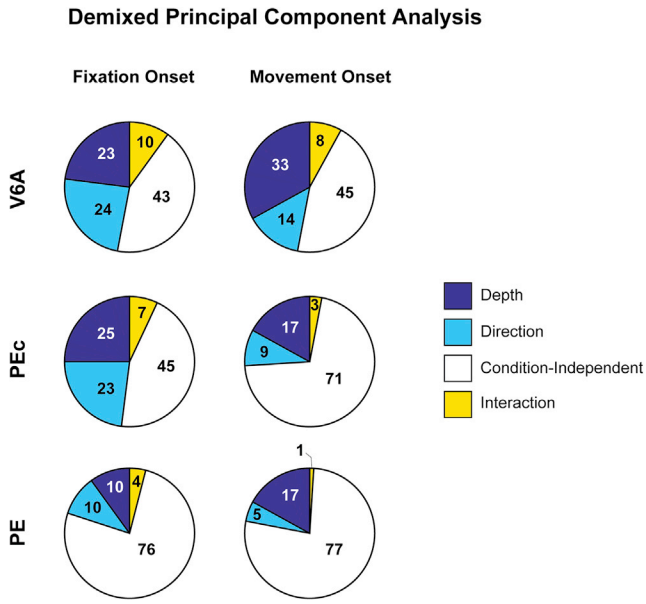

Figure 5. Population activity variance explained by depth and direction

Demixed principal-component analysis: pie charts showing the variance of the individual demixed principal components (depth, blue; direction, light blue; interaction, yellow; condition independent, white) in each area, aligned at fixation onset (left) and movement onset (right). Condition-independent components were significantly different in size between V6A and PE in both time intervals (two-sample proportion binomial test, $p < 0.0001$).

(8%–10%), followed by PEc (37%) and then PE (1%–4%). This finding parallels the results of tuning analyses on single cells (Figure 2), where the highest and lowest convergence of depth and direction signals was observed for V6A and PE, respectively. Despite this trend, the very low percentage of interaction component variance in PE suggests that depth and direction signals are sent separately from PE to the downstream areas. In sum, dPCA revealed interesting trends among the three areas: at early task stages, population activity variance in V6A and PEc showed very similar distributions that were quite different from that of PE, whereas around movement, PEc was much more similar to PE compared with V6A. In the same period, the depth accounted for twice as much of the population variance in V6A compared with the other two areas.

DISCUSSION

Here, we compared depth and direction signals during several phases of an instructed-delay fixate-to-reach task in three areas of the PPC. Given the ongoing debate in psychophysical literature for independent vs. joint control of reach depth and direction, here we compared these signals across the PPC in the same monkey. Our findings further support the two schemes of anatomical and temporal segregation of depth and direction signals reported previously and moreover suggest a gradual parcellation of depth and direction information in the PPC.

Several lines of evidence have demonstrated an AP organization of the primate PPC, with anatomical and functional trends. Anterior areas like PE rely primarily on somatosensory input (Bakola et al., 2013; Padberg et al., 2019), whereas visual inputs are stronger in posterior sectors like V6A and medial intraparietal (MIP) area (Bakola et al., 2017; Gamberini et al., 2009; Passarelli et al., 2011). In addition, these areas are located across the border between Brodmann's areas 5 and 7 (Brodmann, 1909), thus belonging to different neuroanatomical domains: areas V6A and PEc in Brodmann's area 7 and PE in Brodmann's area 5 (Gamberini et al., 2020).

There is evidence that the caudal PPC areas V6A and MIP are more involved in visuospatial processing and encode the target and/or the endpoint of the reaching movement, whereas anterior sectors like PE primarily implement the movement plan (Breveglieri et al., 2014; Cui and Andersen, 2011; Hadjidimitrakis et al., 2020; Li and Cui, 2013). Consistent with this, reach targets are encoded in eye- or body-centered coordinates in MIP, PEc, and V6A (Batista et al., 1999; Bosco et al., 2016; Chang and Snyder, 2012; Hadjidimitrakis et al., 2017, 2020; Pesaran et al., 2006; Piserchia et al., 2017), whereas most PE neurons use a hand-centered coordinate system (Bremner and Andersen, 2012; Buneo et al., 2002; Ferraina et al., 2009). Despite these trends, it is hard to summarize a large number of studies on frames of reference (RFs) with different experimental setups. Moreover, there are no clear-cut differences between the PPC areas, and even in the same area there is high heterogeneity of RFs (e.g., Chang and Snyder, 2010). In addition to these trends, we report here that PPC areas differ in the degree they combine depth and direction information, a finding that might be related to the anatomical and functional gradients mentioned above (Figure 6). Behavioral and computational data suggest that, during arm movement in depth, proprioceptive inputs could be more informative, as movements in depth are linked to larger differences in joint angles compared with movements in a frontal plane, whereas vision is more important for monitoring errors in coding reach direction (van Beers et al., 1998, 2002, 2004; Monaco et al., 2010; Sainburg et al., 2003). Areas V6A and PEc, which integrate visual and proprioceptive inputs (Bakola et al., 2010; Gamberini et al., 2009), are more likely to combine depth and direction signals compared with PE, which mostly relies on proprioception (Bakola et al., 2013). This is in line with our results showing that a large proportion of PE neurons tuned only in depth were recruited during movement (Figure 2). Similarly, studies in PE and in primary somatosensory cortex reported increased numbers of neurons modulated during active or passive hand displacements in depth compared with the azimuth and elevation (Lacquaniti et al., 1995; Tillery et al., 1996).

The dPCA analysis revealed that the depth/direction interaction represented a small proportion of the population variance (up to 10%; Figure 5), thereby suggesting an independent readout of these signals at the population level. Although this result might seem at odds with the substantial convergence of depth and direction in V6A and PEc, a similar segregation at the population response was found in the human PPC (area AIP) for reaching and grasping (Zhang et al., 2017). This functional separation of the task variables in the population activity is a common computational principle in associative cortical areas that might enable a faster and more accurate processing of single task features in downstream areas.

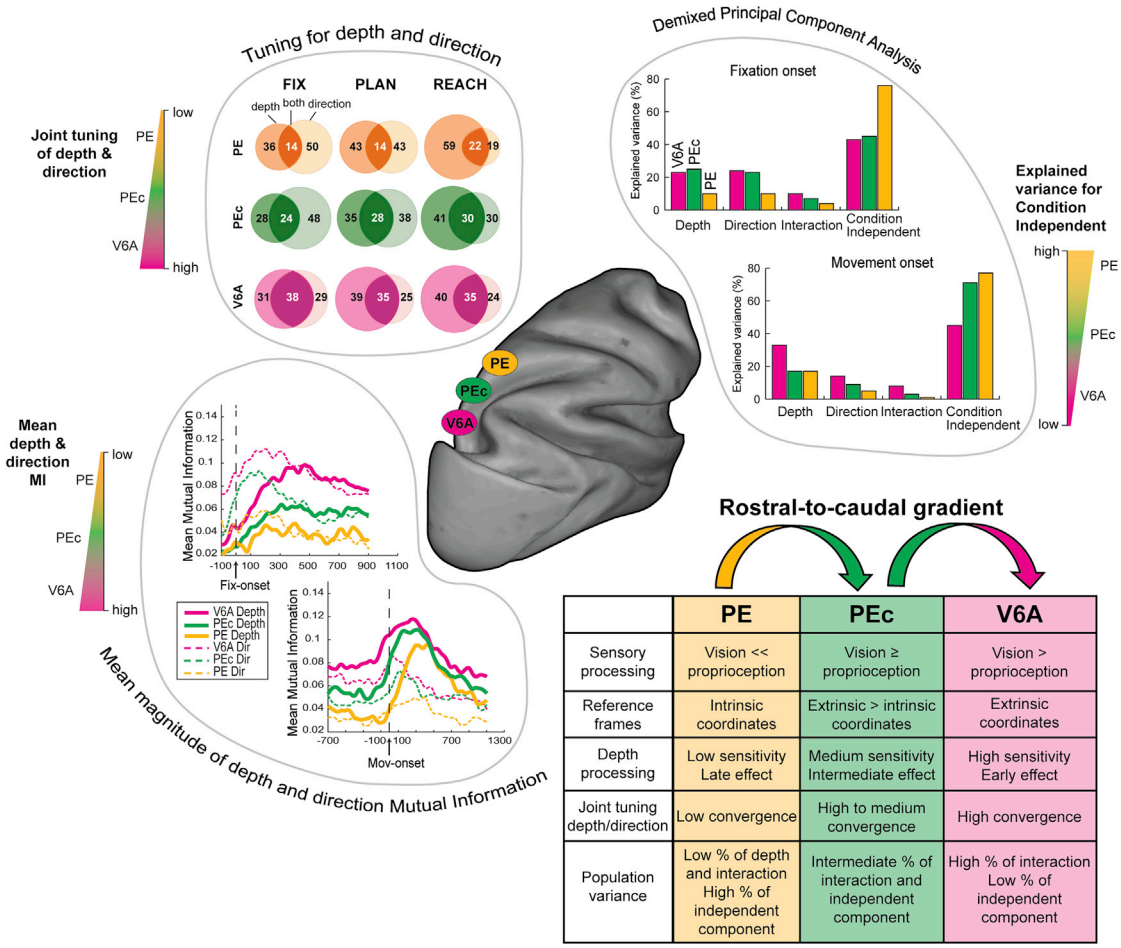

	PE	PEc	V6A
Sensory processing	Vision << proprioception	Vision ≥ proprioception	Vision > proprioception
Reference frames	Intrinsic coordinates	Extrinsic > intrinsic coordinates	Extrinsic coordinates
Depth processing	Low sensitivity Late effect	Medium sensitivity Intermediate effect	High sensitivity Early effect
Joint tuning depth/direction	Low convergence	High to medium convergence	High convergence
Population variance	Low % of depth and interaction High % of independent component	Intermediate % of interaction and independent component	High % of interaction Low % of independent component

Figure 6. Parietal cortex trends in the coding of 3D space

The rostral-to-caudal gradient (i.e., from PE to V6A) in the increased convergence of depth and direction effects, the mutual information, and the proportion of the population activity variance are explained by these two parameters.

The largely segregated processing of depth and direction information in PE could also be viewed in light of a hierarchical organization in the PPC reaching network. In this regard, it should be noted that PE, different from PEc and V6A, is directly connected to the primary motor cortex (Bakola et al., 2013; Johnson et al., 1996; Jones et al., 1978; Strick and Kim, 1978), This hierarchical organization could also hint at a serial processing of depth and direction information in a caudal-to-rostral manner, i.e., from V6A to PE. Our data suggest that this might be the case for depth processing during the arm movement period, since we found earlier peaks in MI both in single cells and in the population average in V6A compared with PEc, which, in turn, showed earlier peaks in MI compared with PE. Notably, this trend was not observed for directional MI, thereby suggesting a rather distributed processing for that variable.

A likely source of direction signals in the PPC is the dorsal premotor cortex (PMd), where a much stronger effect of movement direction with respect to movement distance/amplitude has been reported well before the onset of arm movement in several studies, and this directional tuning was maintained during the movement execution period, when distance processing also increased (Churchland and Shenoy, 2007; Fu et al., 1993, 1995; Messier and Kalaska, 2000). This directional information could be routed posteriorly and thus become available simultaneously to the various PPC sectors through parallel, topographically organized frontoparietal projections that connect rostral and caudal PMd sectors with caudal and rostral PPC, respectively (Bakola et al., 2010, 2013; Gamberini et al., 2009; Johnson et al., 1996). Regarding distance, despite different task configurations in the above PMd studies, in all of them distance signals during movement were processed almost exclusively in conjunction with direction information. This finding is in contrast to the present results from the medial PPC showing substantial neural populations coding only for reach depth information. In addition, a recent reaching study in 2D space that employed dimensionality reduction methods also demonstrated limited resources for reach distance compared with direction processing in the PMd population response (Even-Chen et al., 2019). In line with the above evidence, a human imaging study reported increased sensitivity for reach distance in the parietal compared

with the frontal cortex (Fabbri et al., 2012). The involvement of medial PPC in the encoding of reach distance was first reported in a human case study (Holmes and Horrax, 1919). These observations are in agreement with present results and support a common framework of depth and direction processing in human and nonhuman primates.

The present findings could also be useful to reconcile several findings from lesion and psychophysics experiments. Lesion studies in parietal cortex (Baylis and Baylis, 2001; Danckert et al., 2009; Darling et al., 2001; Schaadt et al., 2015) reported larger effects in depth specification than in direction, and these observations have contributed to the widely accepted model that the two features are specified by distinct circuits and/or populations (Crawford et al., 2011). Based on our findings, we suggest that this model would benefit from a revision considering that the same effects can be produced by overlapping depth and direction populations that show high sensitivity to distance, which peaks during visuospatial processing and movement preparation (i.e., in V6A) and decreases toward execution (i.e., in PEc and PE). In the same vein, in several psychophysics studies where arm movements in 3D were performed, the variability of endpoints was found to be larger along the depth axis compared with the direction axis (Apker et al., 2010; Gordon et al., 1994; McIntyre et al., 1997). This finding could be explained by the lower depth sensitivity of area PE and, to a lesser degree, of PEc, which are more involved in the execution phases of the movement.There again, human data are in line with present findings and further point to a common framework of depth and direction signal processing in human and nonhuman primates.

Limitations of the study

A limitation of the present study is that reaches were always performed toward foveated targets, so we cannot determine the frame of reference. However, we believe that the different trends in distance and direction processing between the three parietal areas could be related to the reference frame transformations. The difference in the degree of convergence of depth and direction information between them might be related to the different representations of movement (Crawford et al., 2011; Flanders et al., 1992). In V6A and PEc, which show strong tuning in all task phases, depth and direction are expected to be defined mostly in extrinsic reference frames (eye or body centered), so they are more likely to be combined. However, in PE, which is more active during and after the movement, depth and direction signals are also referred to the intrinsic coordinates of the elbow and shoulder joint angles and thus are expected to be more independent. Another caveat of our study, also related to the frames of reference, is the fact that, in our task configuration, the near targets were always associated with larger elevation angles with respect to the intermediate and far targets. Accordingly, the distance effects we reported here could be due to the different elevation angles while the arm moves. The issue of reference frames has been addressed in previous studies by our group focused on spatial representations in V6A (Hadjidimitrakis et al., 2014b) and PEc (Piserchia et al., 2017). Those analyses (e.g., Figure 3 in Hadjidimitrakis et al., 2014b) suggested predominant body-centered representations of target locations during movement that imply a minor effect of elevation angle. Similarly for PE, Lacquaniti et al. (1995) reported that target distance was two times stronger with respect to target elevation angle during arm reaching and static posture. It should be noted that in that study, in contrast to ours, both upward and downward arm movements were performed. Accordingly, the elevation effects are expected to be weaker in our experiments.

Another limitation of our study is the fact that the two dimensions of space (depth and direction) we studied were not equivalent. For example, the differences we found could be attributed to the fact that in our experimental setup the depth range explored included most of the possible depths, whereas tested directions covered a smaller fraction of directional space. Although we cannot exclude this explanation, there are several lines of evidence that argue against it. For instance, we did not find the influence of depth to be stronger than the direction influence in the fixation epoch. In addition, although the range of explored directions is small (30°), it comprises most of the space where the gaze and hands interact with objects in everyday life.

In conclusion, our study provides direct evidence for hierarchical control of depth information in the parietal cortex and a gradient of integrated versus independent coding of direction and depth signals. Furthermore, it highlights the importance of anatomical and functional gradients in the PPC that enable flexible spatial and motor representations. Future experiments combining inactivation and simultaneous recording from parietal, premotor, and motor cortex will further provide a comprehensive ‘‘road map’’ of 3D motor control across the cortex.

STAR★METHODS

Detailed methods are provided in the online version of this paper and include the following:

- KEY RESOURCES TABLE
- RESOURCE AVAILABILITY
  - Lead contact
  - Materials availability
  - Data and code availability
- EXPERIMENTAL MODEL AND SUBJECT DETAILS
- METHOD DETAILS
  - Data recording and experimental design
- QUANTIFICATION AND STATISTICAL ANALYSIS
  - ANOVA and spike density function
  - Mutual information
  - Gradient and separability analysis
  - Demixed principal component analysis

SUPPLEMENTAL INFORMATION

Supplemental information can be found online at https://doi.org/10.1016/j.celrep.2022.111608.

ACKNOWLEDGMENTS

We thank Dr. L. Passarelli and Prof. M. Gamberini for assistance in the reconstruction of the penetrations, Drs. F. Bertozzi and G. Dal Bo for help during recordings, and Mr. M. Verdosci and Mr. F. Campisi for help with setting up the experimental apparatus. This work was supported by grants from the

Ministero dell'Università e della Ricerca (2017KZNZLN), the Fondazione Cassa di Risparmio di Bologna (Bando Internazionalizzazione), and European Union-funded projects H2020-MSCA-734227-PLATYPUS, H2020-EIC-FETPROACT-2019-951910-MAIA, and HumanE-AI-Net-952026.

AUTHOR CONTRIBUTIONS

Conceptualization, K.H. and P.F.; data curation management activities, K.H. and M.D.V.; formal analysis application, K.H. and M.D.V.; funding acquisition, P.F.; investigation conduct, K.H., M.D.V., and M.F.; methodology development or design of methodology, K.H., M.D.V., and M.G.; project administration management, P.F.; resources provision of study materials, P.F.; software programming, software development, K.H., M.D.V., M.G., and M.F.; supervision oversight, P.F.; validation verification, P.F.; visualization preparation, M.D.V. and K.H.; writing – original draft, K.H. and M.D.V.; writing – review & editing, K.H., M.D.V, M.F., M.G., and P.F.

DECLARATION OF INTERESTS

The authors declare no competing interests.

INCLUSION AND DIVERSITY

We support inclusive, diverse, and equitable conduct of research.

Received: July 29, 2021
Revised: July 16, 2022
Accepted: October 14, 2022
Published: November 8, 2022

REFERENCES

Andersen, R.A., Andersen, K.N., Hwang, E.J., and Hauschild, M. (2014). Optic ataxia: from Balint's syndrome to the parietal reach region. Neuron *81*, 967–983.

Apker, G.A., and Buneo, C.A. (2012). Contribution of execution noise to arm movement variability in three-dimensional space. J. Neurophysiol. *107*, 90–102.

Apker, G.A., Darling, T.K., and Buneo, C.A. (2010). Interacting noise sources shape patterns of arm movement variability in three-dimensional space. J. Neurophysiol. *104*, 2654–2666.

Bagesteiro, L.B., Sarlegna, F.R., and Sainburg, R.L. (2006). Differential influence of vision and proprioception on control of movement distance. Exp. Brain Res. *171*, 358–370.

Bakola, S., Gamberini, M., Passarelli, L., Fattori, P., and Galletti, C. (2010). Cortical connections of parietal field PEc in the macaque: linking vision and somatic sensation for the control of limb action. Cereb. Cortex *20*, 2592–2604.

Bakola, S., Passarelli, L., Gamberini, M., Fattori, P., and Galletti, C. (2013). Cortical connectivity suggests a role in limb coordination for macaque area PE of the superior parietal cortex. J. Neurosci. *33*, 6648–6658.

Bakola, S., Passarelli, L., Huynh, T., Impieri, D., Worthy, K.H., Fattori, P., Galletti, C., Burman, K.J., and Rosa, M.G.P. (2017). Cortical afferents and myeloarchitecture distinguish the medial intraparietal area (MIP) from neighboring subdivisions of the macaque cortex. ENeuro *4*.

Barany, D.A., Della-Maggiore, V., Viswanathan, S., Cieslak, M., and Grafton, S.T. (2014). Feature interactions enable decoding of sensorimotor transformations for goal-directed movement. J. Neurosci. *34*, 6860–6873.

Batista, A.P., Buneo, C.A., Snyder, L.H., and Andersen, R.A. (1999). Reach plans in eyecentered coordinates. Science *285*, 257–260.

Baylis, G.C., and Baylis, L.L. (2001). Visually misguided reaching in Balint's syndrome. Neuropsychologia *39*, 865–875.

van Beers, R.J., Sittig, A.C., and Denier van der Gon, J.J. (1998). The precision of proprioceptive position sense. Exp. Brain Res. *122*, 367–377.

van Beers, R.J., Wolpert, D.M., and Haggard, P. (2002). When feeling is more important than seeing in sensorimotor adaptation. Curr. Biol. *12*, 834–837.

van Beers, R.J., Haggard, P., and Wolpert, D.M. (2004). The role of execution noise in movement variability. J. Neurophysiol. *91*, 1050–1063.

Bhat, R.B., and Sanes, J.N. (1998). Cognitive channels computing action distance and direction. J. Neurosci. *18*, 7566–7580.

Bosco, A., Breveglieri, R., Chinellato, E., Galletti, C., and Fattori, P. (2010). Reaching activity in the medial posterior parietal cortex of monkeys is modulated by visual feedback. J. Neurosci. *30*, 14773–14785.

Bosco, A., Breveglieri, R., Hadjidimitrakis, K., Galletti, C., and Fattori, P. (2016). Reference frames for reaching when decoupling eye and target position in depth and direction. Sci. Rep. *6*, 21646.

Bosco, A., Breveglieri, R., Filippini, M., Galletti, C., and Fattori, P. (2019). Reduced neural representation of arm/hand actions in the medial posterior parietal cortex. Sci. Rep. *9*, 936.

Bremner, L.R., and Andersen, R.A. (2012). Coding of the reach vector in parietal area 5d. Neuron *75*, 342–351.

Bremner, L.R., and Andersen, R.A. (2014). Temporal analysis of reference frames in parietal cortex area 5d during reach planning. J. Neurosci. *34*, 5273–5284.

Breveglieri, R., Galletti, C., Dal Bò, G., Hadjidimitrakis, K., and Fattori, P. (2014). Multiple aspects of neural activity during reaching preparation in the medial posterior parietal area V6A. J. Cogn. Neurosci. *26*, 878–895.

Brodmann, K. (1909). Vergleichende Lokalisationslehre der Grosshirnrinde in ihren Prinzipien dargestellt auf Grund des Zellenbaues (Wellcome Collection).

Buneo, C.A. (2011). Analyzing neural responses with vector fields. J. Neurosci. Methods *197*, 109–117.

Buneo, C.A., and Andersen, R.A. (2012). Integration of target and hand position signals in the posterior parietal cortex: effects of workspace and hand vision. J. Neurophysiol. *108*, 187–199.

Buneo, C.A., Jarvis, M.R., Batista, A.P., and Andersen, R.A. (2002). Direct visuomotor transformations for reaching. Nature *416*, 632–636.

Chang, S.W.C., and Snyder, L.H. (2010). Idiosyncratic and systematic aspects of spatial representations in the macaque parietal cortex. Proc. Natl. Acad. Sci. USA *107*, 7951–7956.

Chang, S.W.C., and Snyder, L.H. (2012). The representations of reach endpoints in posterior parietal cortex depend on which hand does the reaching. J. Neurophysiol. *107*, 2352–2365.

Chen, J., Reitzen, S.D., Kohlenstein, J.B., and Gardner, E.P. (2009). Neural representation of hand kinematics during prehension in posterior parietal cortex of the macaque monkey. J. Neurophysiol. *102*, 3310–3328.

Churchland, M.M., and Shenoy, K.V. (2007). Temporal complexity and heterogeneity of single-neuron activity in premotor and motor cortex. J. Neurophysiol. *97*, 4235–4257.

Churchland, M.M., Santhanam, G., and Shenoy, K.V. (2006). Preparatory activity in premotor and motor cortex reflects the speed of the upcoming reach. J. Neurophysiol. *96*, 3130–3146.

Crawford, J.D., Henriques, D.Y.P., and Medendorp, W.P. (2011). Three-dimensional transformations for goal-directed action. Annu. Rev. Neurosci. *34*, 309–331.

Cui, H., and Andersen, R.A. (2011). Different representations of potential and selected motor plans by distinct parietal areas. J. Neurosci. *31*, 18130–18136.

Danckert, J., Goldberg, L., and Broderick, C. (2009). Damage to superior parietal cortex impairs pointing in the sagittal plane. Exp. Brain Res. *195*, 183–191.

Darling, W.G., Rizzo, M., and Butler, A.J. (2001). Disordered sensorimotor transformations for reaching following posterior cortical lesions. Neuropsychologia *39*, 237–254.

Diomedi, S., Vaccari, F.E., Filippini, M., Fattori, P., and Galletti, C. (2020). Mixed selectivity in macaque medial parietal cortex during eye-hand reaching. iScience *23*, 101616.

Efron, B., and Tibshirani, R.J. (1993). An Introduction to the Bootstrap (Springer US).

Even-Chen, N., Stavisky, S.D., Kao, J.C., Ryu, S.I., and Shenoy, K.V. (2017). Augmenting intracortical brain-machine interface with neurally driven error detectors. J. Neural. Eng. *14*, 066007.

Even-Chen, N., Sheffer, B., Vyas, S., Ryu, S.I., and Shenoy, K.V. (2019). Structure and variability of delay activity in premotor cortex. PLoS Comput. Biol. *15*, e1006808.

Fabbri, S., Caramazza, A., and Lingnau, A. (2012). Distributed sensitivity for movement amplitude in directionally tuned neuronal populations. J. Neurophysiol. *107*, 1845–1856.

Fattori, P., Breveglieri, R., Bosco, A., Gamberini, M., and Galletti, C. (2017). Vision for prehension in the medial parietal cortex. Cereb. Cortex *27*, 1149–1163.

Ferraina, S., Battaglia-Mayer, A., Genovesio, A., Marconi, B., Onorati, P., and Caminiti, R. (2001). Early coding of visuomanual coordination during reaching in parietal area PEc. J. Neurophysiol. *85*, 462–467.

Ferraina, S., Brunamonti, E., Giusti, M.A., Costa, S., Genovesio, A., and Caminiti, R. (2009). Reaching in depth: hand position dominates over binocular eye position in the rostral superior parietal lobule. J. Neurosci. *29*, 11461–11470.

Filimon, F., Nelson, J.D., Huang, R.-S., and Sereno, M.I. (2009). Multiple parietal reach regions in humans: cortical representations for visual and proprioceptive feedback during online reaching. J. Neurosci. *29*, 2961–2971.

Flanders, M., Tillery, S.I.H., and Soechting, J.F. (1992). Early stages in a sensorimotor transformation. Behav. Brain Sci. *15*, 309–320.

Fu, Q.G., Suarez, J.I., and Ebner, T.J. (1993). Neuronal specification of direction and distance during reaching movements in the superior precentral premotor area and primary motor cortex of monkeys. J. Neurophysiol. *70*, 2097–2116.

Fu, Q.G., Flament, D., Coltz, J.D., and Ebner, T.J. (1995). Temporal encoding of movement kinematics in the discharge of primate primary motor and premotor neurons. J. Neurophysiol. *73*, 836–854.

Gamberini, M., Dal Bò, G., Breveglieri, R., Briganti, S., Passarelli, L., Fattori, P., and Galletti, C. (2018). Sensory properties of the caudal aspect of the macaque's superior parietal lobule. Brain Struct. Funct. *223*, 1863–1879.

Gamberini, M., Passarelli, L., Fattori, P., Zucchelli, M., Bakola, S., Luppino, G., and Galletti, C. (2009). Cortical connections of the visuomotor parietooccipital area V6Ad of the macaque monkey. J. Comp. Neurol. *513*, 622–642.

Gamberini, M., Galletti, C., Bosco, A., Breveglieri, R., and Fattori, P. (2011). Is the medial posterior parietal area V6A a single functional area? J. Neurosci. *31*, 5145–5157.

Gamberini, M., Passarelli, L., Fattori, P., and Galletti, C. (2020). Structural connectivity and functional properties of the macaque superior parietal lobule. Brain Struct. Funct. *225*, 1349–1367.

Ghodrati, M., Alwis, D.S., and Price, N.S.C. (2016). Orientation selectivity in rat primary visual cortex emerges earlier with low-contrast and high-luminance stimuli. Eur. J. Neurosci. *44*, 2759–2773.

Ghodrati, M., Zavitz, E., Rosa, M.G.P., and Price, N.S.C. (2019). Contrast and luminance adaptation alter neuronal coding and perception of stimulus orientation. Nat. Commun. *10*, 941.

Gordon, J., Ghilardi, M.F., and Ghez, C. (1994). Accuracy of planar reaching movements. I.Independence of direction and extent variability. Exp. Brain Res. *99*, 97–111.

Hadjidimitrakis, K., Bertozzi, F., Breveglieri, R., Bosco, A., Galletti, C., and Fattori, P. (2014a). Common neural substrate for processing depth and direction signals for reaching in the monkey medial posterior parietal cortex. Cereb. Cortex *24*, 1645–1657.

Hadjidimitrakis, K., Bertozzi, F., Breveglieri, R., Fattori, P., and Galletti, C. (2014b). Bodycentered, mixed, but not hand-centered coding of visual targets in the medial posterior parietal cortex during reaches in 3D space. Cereb. Cortex *24*, 3209–3220.

Hadjidimitrakis, K., Dal Bo', G., Breveglieri, R., Galletti, C., and Fattori, P. (2015). Overlapping representations for reach depth and direction in caudal superior parietal lobule of macaques. J. Neurophysiol. *114*, 2340–2352.

Hadjidimitrakis, K., Bertozzi, F., Breveglieri, R., Galletti, C., and Fattori, P. (2017). Temporal stability of reference frames in monkey area V6A during a reaching task in 3D space. Brain Struct. Funct. *222*, 1959–1970.

Hadjidimitrakis, K., Bakola, S., Wong, Y.T., and Hagan, M.A. (2019). Mixed spatial and movement representations in the primate posterior parietal cortex. Front. Neural Circuits *13*, 15.

Hadjidimitrakis, K., Ghodrati, M., Breveglieri, R., Rosa, M.G.P., and Fattori, P. (2020). Neural coding of action in three dimensions: task- and time-invariant reference frames for visuospatial and motor-related activity in parietal area V6A. J. Comp. Neurol. *528*, 3108–3122.

Hawkins, K.M., Sayegh, P., Yan, X., Crawford, J.D., and Sergio, L.E. (2013). Neural activity in superior parietal cortex during rule-based visual-motor transformations. J. Cogn. Neurosci. *25*, 436–454.

Holmes, G., and Horrax, G. (1919). Disturbances of spatial orientation and visual attention, with loss of stereoscopic vision. Arch. Neurol. Psychiatry *1*, 385–407.

Husain, M., and Nachev, P. (2007). Space and the parietal cortex. Trends Cogn. Sci. *11*, 30–36.

Johnson, P.B., Ferraina, S., Bianchi, L., and Caminiti, R. (1996). Cortical networks for visual reaching: physiological and anatomical organization of frontal and parietal lobe arm regions. Cereb. Cortex *6*, 102–119.

Jones, E.G., Coulter, J.D., and Hendry, S.H. (1978). Intracortical connectivity of architectonic fields in the somatic sensory, motor and parietal cortex of monkeys. J. Comp. Neurol. *181*, 291–347.

Kobak, D., Brendel, W., Constantinidis, C., Feierstein, C.E., Kepecs, A., Mainen, Z.F., Qi, X.L., Romo, R., Uchida, N., and Machens, C.K. (2016). Demixed principal component analysis of neural population data. Elife *5*, 109899–e11037.

Kutz, D.F., Marzocchi, N., Fattori, P., Cavalcanti, S., and Galletti, C. (2005). Real-time supervisor system based on trinary logic to control experiments with behaving animals and humans. J. Neurophysiol. *93*, 3674–3686.

Lacquaniti, F., Guigon, E., Bianchi, L., Ferraina, S., and Caminiti, R. (1995). Representing spatial information for limb movement: role of area 5 in the monkey. Cereb. Cortex *5*, 391–409.

de Lafuente, V., Jazayeri, M., and Shadlen, M.N. (2015). Representation of accumulating evidence for a decision in two parietal areas. J. Neurosci. *35*, 4306–4318.

Lefrançois, C., and Messier, J. (2019). Adaptation and spatial generalization to a triaxial visuomotor perturbation in a virtual reality environment. Exp. Brain Res. *237*, 793–803.

Lehmann, S.J., and Scherberger, H. (2013). Reach and gaze representations in macaque parietal and premotor grasp areas. J. Neurosci. *33*, 7038–7049.

Li, Y., and Cui, H. (2013). Dorsal parietal area 5 encodes immediate reach in sequential arm movements. J. Neurosci. *33*, 14455–14465.

Luppino, G., Ben Hamed, S., Gamberini, M., Matelli, M., and Galletti, C. (2005). Occipital (V6) and parietal (V6A) areas in the anterior wall of the parieto-occipital sulcus of the macaque: a cytoarchitectonic study. Eur. J. Neurosci. *21*, 3056–3076.

Marzocchi, N., Breveglieri, R., Galletti, C., and Fattori, P. (2008). Reaching activity in parietal area V6A of macaque: eye influence on arm activity or retinocentric coding of reaching movements? Eur. J. Neurosci. *27*, 775–789.

McGuire, L.M.M., and Sabes, P.N. (2011). Heterogeneous representations in the superior parietal lobule are common across reaches to visual and proprioceptive targets. J. Neurosci. *31*, 6661–6673.

McIntyre, J., Stratta, F., and Lacquaniti, F. (1997). Viewer-centered frame of reference for pointing to memorized targets in three-dimensional space. J. Neurophysiol. *78*, 1601–1618.

Medendorp, W.P., Tweed, D.B., and Crawford, J.D. (2003). Motion parallax is computed in the updating of human spatial memory. J. Neurosci. *23*, 8135–8142.

Messier, J., and Kalaska, J.F. (1999). Comparison of variability of initial kinematics and endpoints of reaching movements. Exp. Brain Res. *125*, 139–152.

Messier, J., and Kalaska, J.F. (2000). Covariation of primate dorsal premotor cell activity with direction and amplitude during a memorized-delay reaching task. J. Neurophysiol. *84*, 152–165.

Michaels, J.A., and Scherberger, H. (2018). Population coding of grasp and laterality-related information in the macaque fronto-parietal network. Sci. Rep. *8*, 1710.

Michaels, J.A., and Scherberger, H. (2018). Population coding of grasp and laterality-related information in the macaque fronto-parietal network. Sci. Rep. *8*.

Monaco, S., Króliczak, G., Quinlan, D.J., Fattori, P., Galletti, C., Goodale, M.A., and Culham, J.C. (2010). Contribution of visual and proprioceptive information to the precision of reaching movements. Exp. Brain Res. *202*, 15–32.

Naselaris, T., Merchant, H., Amirikian, B., and Georgopoulos, A.P. (2006). Large-Scale organization of preferred directions in the motor cortex. I. Motor cortical hyperacuity for forward reaching. J. Neurophysiol. *96*, 3231–3236.

Padberg, J., Cooke, D.F., Cerkevich, C.M., Kaas, J.H., and Krubitzer, L. (2019). Cortical connections of area 2 and posterior parietal area 5 in macaque monkeys. J. Comp. Neurol. *527*, 718–737.

Pandya, D.N., and Seltzer, B. (1982). Intrinsic connections and architectonics of posterior parietal cortex in the rhesus monkey. J. Comp. Neurol. *204*, 196–210.

Panzeri, S., Senatore, R., Montemurro, M.A., and Petersen, R.S. (2007). Correcting for the sampling bias problem in spike train information measures. J. Neurophysiol. *98*, 1064–1072.

Passarelli, L., Rosa, M.G.P., Gamberini, M., Bakola, S., Burman, K.J., Fattori, P., and Galletti, C. (2011). Cortical connections of area V6Av in the macaque: a visual-input node to the eye/hand coordination system. J. Neurosci. *31*, 1790–1801.

Van Pelt, S., and Medendorp, W.P. (2008). Updating target distance across eye movements in depth. J. Neurophysiol. *99*, 2281–2290.

Peña, J.L., and Konishi, M. (2001). Auditory spatial receptive fields created by multiplication. Science *292*, 249–252.

Pesaran, B., Nelson, M.J., and Andersen, R.A. (2006). Dorsal premotor neurons encode the relative position of the hand, eye, and goal during reach planning. Neuron *51*, 125–134.

Pesaran, B., Nelson, M.J., and Andersen, R.A. (2010). A relative position code for saccades in dorsal premotor cortex. J. Neurosci. *30*, 6527–6537.

Piserchia, V., Breveglieri, R., Hadjidimitrakis, K., Bertozzi, F., Galletti, C., and Fattori, P. (2017). Mixed body/hand reference frame for reaching in 3D space in macaque parietal area PEc. Cereb. Cortex *27*, 1976–1990.

Sainburg, R.L., Lateiner, J.E., Latash, M.L., and Bagesteiro, L.B. (2003). Effects of altering initial position on movement direction and extent. J. Neurophysiol. *89*, 401–415.

Sarlegna, F.R., and Blouin, J. (2010). Visual guidance of arm reaching: online adjustments of movement direction are impaired by amplitude control. J. Vis. *10*, 24.

Schaadt, A.K., Brandt, S.A., Kraft, A., and Kerkhoff, G. (2015). Holmes and Horrax (1919) revisited: impaired binocular fusion as a cause of "flat vision" after right parietal brain damage - a case study. Neuropsychologia *69*, 31–38.

Shi, Y., Apker, G., and Buneo, C.A. (2013). Multimodal representation of limb endpoint position in the posterior parietal cortex. J. Neurophysiol. *109*, 2097–2107.

Soechting, J.F., and Flanders, M. (1989). Sensorimotor representations for pointing to targets in three-dimensional space. J. Neurophysiol. *62*, 582–594.

Strick, P.L., and Kim, C.C. (1978). Input to primate motor cortex from posterior parietal cortex (area 5). I. Demonstration by retrograde transport. Brain Res. *157*, 325–330.

Tillery, S.I., Soechting, J.F., and Ebner, T.J. (1996). Somatosensory cortical activity in relation to arm posture: nonuniform spatial tuning. J. Neurophysiol. *76*, 2423–2438.

Tramper, J.J., and Gielen, C.C.A.M. (2011). Visuomotor coordination is different for different irections in three-dimensional space. J. Neurosci. *31*, 7857–7866.

Vindras, P., Desmurget, M., and Viviani, P. (2005). Error parsing in visuomotor pointing reveals independent processing of amplitude and direction. J. Neurophysiol. *94*, 1212–1224.

De Vitis, M., Breveglieri, R., Hadjidimitrakis, K., Vanduffel, W., Galletti, C., and Fattori, P. (2019). The neglected medial part of macaque area PE: segregated processing of reach depth and direction. Brain Struct. Funct. *224*, 2537–2557.

De Vitis, M., Tabanelli, M., Breveglieri, R., Filippini, M., Galletti, C., and Fattori, P. (2022). The superior parietal lobule of macaque monkey: relative influence of gaze and static arm position during reaching. ENeuro *9*.

Wijdenes, L.O., Brenner, E., and Smeets, J.B.J. (2013). Comparing online adjustments to distance and direction in fast pointing movements. J. Mot. Behav. *45*, 395–404.

Zhang, C.Y., Aflalo, T., Revechkis, B., Rosario, E.R., Ouellette, D., Pouratian, N., and Andersen, R.A. (2017). Partially mixed selectivity in human posterior parietal association cortex. Neuron *95*, 697–708.e4.

STAR★METHODS

KEY RESOURCES TABLE

REAGENT or RESOURCE	SOURCE	IDENTIFIER
Experimental models: Organisms/strains		
Long-tailed Macaques (Macaca fascicularis)	University of Bologna	N/A
Software and algorithms		
MATLAB	MathWorks	https://ch.mathworks.com/products/matlab.html?s_tid = hp_products_matlab
dPCA	https://elifesciences.org/articles/10989#s4	http://github.com/machenslab/dPCA
Other		
5-channel MiniMatrix	Thomas recording	https://www.thomasrecording.com/5-electrode-mini-matrix
ETL-200 Eye tracking system	ISCAN, Inc	http://iscaninc.com/standard-systems

RESOURCE AVAILABILITY

Lead contact

Further information and requests for resources should be directed to and will be fulfilled by the lead contact, Kostas Hadjidimitrakis (kon.chatzidimitrakis@unibo.it).

Materials availability

This study did not generate new unique reagents.

Data and code availability

- The dataset supporting the current study are available from the lead contact upon reasonable request.
- This paper does not report original code.
- Any additional information required to reanalyze the data reported in this work paper is available from the lead contact upon request.

EXPERIMENTAL MODEL AND SUBJECT DETAILS

Two male macaque monkeys (*Macaca fascicularis*, monkeys M1 and M2) with a weight ranging between 4 and 4.6 kg were involved in this study. The experiment was performed in accordance with the guidelines of EU Directives (86/609/EEC; 2010/63/EU) and Italian national laws (D.L. 116-92, D.L. 26-2014) on the protection of animals used for scientific purposes. Protocols were approved by the Animal-Welfare Body of the University of Bologna.

METHOD DETAILS

Data recording and experimental design

During training and recording sessions, particular attention was paid to any behavioral and clinical sign of pain or distress. For detailed surgical and electrophysiological procedures, see Gamberini et al., 2018. In brief, we performed multiple electrode penetrations using a five-channel multielectrode recording system (5-channel MiniMatrix, Thomas Recording). The signals from the electrodes were amplified (at a gain of 10,000) and filtered (bandpass between 0.5 and 5 kHz). The action potentials recorded in each channel were isolated using a waveform discriminator (Multi Spike Detector; Alpha Omega Engineering) and were sampled at 100 kHz.

Reconstruction of microelectrode penetrations and the criteria used to recognize V6A, PEc, and PE were in accordance with previous reports (Gamberini et al., 2011; Luppino et al., 2005; Pandya and Seltzer, 1982).

Electrophysiological data were collected while monkeys were performing a fix-to-reach task with the contralateral limb (with respect to the recording hemisphere), in darkness, while maintaining steady fixation of the target. Animals sat in front of a horizontal

panel located at eye level with nine light-emitting diodes (LEDs, 6 mm in diameter) placed at different distances and directions and used both as fixation and reaching targets. The time sequence of the task was identical to the one described in Hadjidimitrakis et al. (2014a, 2015) and De Vitis et al. (2019, 2022). Briefly, a trial began when the monkey pressed a home button (2.5 cm in diameter) placed 4 cm in front of its trunk (HB, Figure 1A). After 1 s, one of the nine LEDs was switched on to green. The monkey had to fixate the LED while keeping the HB button pressed (FIX; Figure 1A, left) and then wait 1.5–2.5 s for a change in the color of the same LED (from green to red) without performing any eye or arm movement (preparation of the movement, PLAN, Figure 1A, center). The color change was the go signal for the animal to release the HB and to start an arm movement toward the target (movement execution, REACH, Figure 1A, right). The monkey then reached the target and held its hand on the target for 0.8–1.2 s. The switching off of the target cued the monkey to release it and to return to the HB, which ended the trial and allowed the monkey to receive its reward. The presentation of stimuli and the animals' performance were monitored using custom software written in Labview (National Instruments), as described previously (Kutz et al., 2005). Eye position signals were controlled by an electronic window (4 × 4°) centered on the fixation target and sampled with 2 cameras (ISCAN, 100Hz), one per eye. If the monkey broke fixation or did not respect the temporal constraints of the task, the trial was aborted. The task was performed in the darkness, in blocks of 90 randomized trials, 10 for each target position.

At the beginning of each recording session, the monkeys were required to perform a calibration task consisting in gazing at targets on a frontal panel placed at a distance of 15 cm from the eyes. For each eye, signals to be used for calibration were extracted during fixation of five LEDs arranged in the shape of a cross, one centrally aligned with the eye's straight-ahead position and four peripherally placed at an angle of ±15° (distance 4 cm) in both the horizontal and vertical directions. From the two individual calibrated eye position signals, we derived the mean of the two eyes (conjugate or version signal) and the difference between the two eyes (disconjugate or vergence signal) using the following equations: version = (R + L)/2 and vergence = L - R, where L and R are the position of the left and right eye, respectively, expressed in degrees of visual angle. The version and vergence values were also used by the LabVIEW software to control the gaze position. In the Fix-to-reach task, the fixation target was always coincident with the reaching target. Given that the target was foveated in all epochs of interest, its depth and direction in visual (eye-centered) and head/body-centered space were equal to the vergence and version angles of the eyes, respectively. In movement (i.e., hand-centered) space, in our setup apart from target direction and depth, there was also the elevation angle. It should be added that these last two parameters were correlated, as nearer/farther targets were associated with larger/smaller elevation angles. Accordingly, it cannot be completely excluded that some elevation effects could have influenced the neural activity (see discussion).

QUANTIFICATION AND STATISTICAL ANALYSIS

All the analyses were performed using customized scripts in MATLAB (Mathworks, Natick, MA, US, RRID: SCR_001622). The neural activity was analyzed by quantifying the discharge in the following three different epochs (Figure 1A): (1) the early fixation epoch (FIX), from 50 ms after the end of the saccade performed to gaze at the LED until 450 ms after it; (2) the preparation epoch (PLAN), the last 500 ms of fixation before the go-signal; and (3) the reach epoch (REACH), from 200 ms before arm movement onset until the end of it, signaled by the pressing of the LED target. From trial to trial, this epoch was of different duration, depending on animal's movement times. We also quantified neural activity in a movement epoch of a fixed duration of 300 ms, from movement onset until 300 ms after it. All analyses were done offline.

ANOVA and spike density function

To quantify the proportion of V6A, PEc and PE neurons modulated by each variable in each epoch, we performed a 2-way analysis of variance (ANOVA). Target depth was defined as the distance of the target from the animal (near, intermediate, far), and target direction as its position with respect to the recording hemisphere (ipsilateral, central, contralateral). We considered that neurons were modulated by a given factor only when the factor's main effect was significant ($p < 0.01$). Given that the target was foveated in all epochs of interest, its depth and direction in space were determined by the vergence and version angles of the eyes, respectively. In addition, we tested for significant tuning at multiple time points *t* using a two-way ANOVA on the spike count in a 200 ms window centered around *t*. This test was repeated in time steps of 50 ms (sliding window ANOVA, $p < 0.01$, Figure 2B). Criteria for significant tuning were the same as for the ANOVA analysis of the fixed time epochs.

Population response of all the recorded cells was calculated as averaged spike density function (SDF). An SDF was calculated (Gaussian kernel, half-width 40 ms) for each neuron included in the analysis and averaged across all the trials for each tested target. We found the peak discharge rate of the preferred condition and used it to normalize the SDF. Population SDF curves representing the activity of the preferred and nonpreferred target positions were constructed by averaging the individually-normalized SDFs of the cells (Marzocchi et al., 2008), aligned at the behavioral event of interest. The maximum response of the preferred condition was used to normalize the SDF within each area and for each behavioral event of alignment. To statistically compare the population SDF curves we employed a permutation test and permuted (10,000 iterations) the data from all 9 positions, then selected a new preferred and nonpreferred condition, and finally compared the sum of squared errors of these two new conditions to the original findings. The intervals of the curve permutation test comparisons varied according to the epoch considered: for FIX, the interval was from 50 to 450 ms after saccade offset; for PLAN, the interval included the last 500 ms of fixation before the go-signal; for REACH, the interval was from 200 ms before the movement onset until the red target LED was reached. In order to enhance the temporal resolution of the

analysis, we divided the data of each time epoch considered in bins of 20 ms and performed the permutation test in each time bin independently.

Mutual information

We quantified the amount of information conveyed by neurons about depth and direction using information-theoretic analysis as reported previously (Ghodrati et al., 2016, 2019). The MI between the spiking activity and depth or directional information was calculated using the following equation:

$$MI_{t,\delta t(\theta,R)} = \Sigma_{\forall\theta} p(\theta) \Sigma_{\forall R} p(R|\theta) \log 2(p(R|\theta)p(R))$$

Where:

$$p(R) = \Sigma \cdot \Sigma p(\theta) p(R|\theta)$$

Where, R is the spike count in a time interval τ (aligned at fixation/movement onset) of width δt; $p(\theta)$ is the probability of presenting depth or direction θ, which is close to uniform in our case (1/3); $p(R)$ is the probability of observing response R evoked across all depth and direction conditions; $p(R|\theta)$ is the conditional probability of observing response R given target depth or direction θ was presented. We also applied a bootstrap-based bias-correction method to have an unbiased estimation of information (Efron and Tibshirani, 1993).

The above calculation was performed twice in 200-ms bins: i) during the early phase, which is the time window between −200 and 1 s after the fixation onset, ii) during the interval encompassing the PLAN and REACH epochs, in the time window between −0.8 before till 1.2 s after the movement onset. Using binned neuronal activity aligned at specific task events, we were able to compare the amplitudes and temporal evolution of the two types of mutual information across the three parietal areas.

Gradient and separability analysis

Gradient analysis was used to assess whether a cell was significantly tuned and, if so, which of the two behavioral variables (depth or direction) exerted a stronger influence on the firing rate of the cell (Buneo, 2011; Buneo and Andersen, 2012). In this analysis the 3 × 3 matrix of mean firing rates was converted (using the MATLAB function 'gradient') into a gradient i.e., a two-dimensional vector field (see also red arrows in the left plots of Figure S4). The directions and lengths of the set of red arrows indicate how the activity changes between matrix elements i.e., when the target depth and the direction position shift. The length of each arrow is numerically calculated as the gradient i.e., a derivative of the firing rate. Put together, they indicate the relative influence of depth and direction position on the activity. For example, in the cell of Figure S4 most of the red arrows point to the left, illustrating the stronger effect of changes in direction (Di) with respect to changes in depth (De). Then in the circular plots to the right of each matrix, we summarized this information into a single resultant angle vector (or field orientation vector) that was computed by summing (vector addition) all the gradient elements i.e., all the individual red arrows. In some cases, matrices could show a symmetrical pattern of red arrows (some arrows pointing to the left/up and others to the right/down) that would cancel out during vector summation. To account for symmetric red arrows, the angles of the red arrows were doubled (e.g., $\pi/2$ was converted to π) before being summed). The result of this summation i.e., the resultant angle, was illustrated on circular plots from 0° to +/−180°. In Figure S2, a-c, each circular plot is shown with the interpretation of the relative strength of direction (Di) and depth (De) position: Di at 0°, De at +/−180°, Di-De at −90°. More specifically, resultant vectors pointing at 0° reflect a left/right pattern of red arrows and indicate a strong effect of target location direction Di, whereas a resultant vector pointing +/−180° an upward/downward pattern and indicate a strong effect of depth De. In Figure S2C resultant vectors with angles of −90° reflect a mixed pattern of red arrows, with Di-De vector is the difference between direction and depth position that can be interpreted as encoding of relative direction-depth encoding. Each matrix was classified as tuned if the resultant length was significantly greater than the resultant length calculated after randomization of the matrix elements (Gradient randomization test). In each single cell, arrow length of the resultant was normalized in unit length before being plotted. Rayleigh's test was used to assess the uniformity of circular histograms for tuned resultant angles ($p < 0.05$, with Bonferroni correction for multiple comparisons).

A sliding window population gradient analysis was also performed for each area to investigate the temporal evolution of population responses along the task progress in more detail. Here the resultant length and orientation of the gradient in each cell tuned in at least one epoch was computed in 300-ms windows that moved in 50 ms steps. Firing rates were aligned to the start of fixation from 500 ms before to 700 ms after it, and to the Key Up signal from 500 ms before, to 700 ms after it. In each area, the mean resultant population vector was computed at each time step. Arrow lengths for the population analysis were averaged (vector summation) within each subpopulation and therefore they were not comparable across subpopulations.

We used singular value decomposition (SVD) to determine whether the response matrix for a neuron in each of the FIX, PLAN and REACH epochs was separable or inseparable for the depth (De) and direction (Di) variable. In a separable response, depth and direction position affect neural activity independently by a multiplicative i.e., gain-like coding mechanism, whereas in an inseparable response this mechanism could not completely reconstruct the neural responses (Bremner and Andersen, 2012, 2014; Peña and Konishi, 2001; Pesaran et al., 2006, 2010). More specifically, in a separable response the firing activity of a neuron shows a gain relationship to a pair of variables:

Firing rate = f(Di).f(De), Alternatively, if the firing activity of a neuron can be described as:

Firing rate = f(De-Di), it means that a neuron shows an inseparable response with De and Di being part of the same function f and cannot be multiplicatively separated. SVD is a method of linear algebra used to reconstruct a general, two-dimensional matrix M containing multivariate data. In theory, an inseparable response could result from more complex patterns (e.g., 'De + Di') not considered here. SVD reduces the matrix M into a weighted sum of products of two independent vectors, termed 'singular vectors'. The relative contribution of the products to the original matrix is quantified by their weights (s1, s2, etc.), named 'singular values'. The method reduces M into another matrix, called N, using the formula:

$$N = USVT$$

where S is a diagonal matrix containing singular values, and U and V are orthogonal matrices containing singular vectors. From the 3 × 3 (Depth x Direction) matrices for each cell and epoch (i.e., the two-dimensional response matrix described above) we calculated the diagonal matrix S that contained the singular values:

$$f(De,\ Di) = s1t1(De)h1(Di) + s2t2(De)h2(Di) + \ldots.$$

If the first singular value is quite large compared to second and rest singular values, then the matrix can be reconstructed only by the first term of the equation above:

$$f(De,\ Di) = s1t1(De)h1(Di)$$

In this case, there is a gain relationship between depth and direction that shows multiplication. If instead the first singular value is not much larger with respect to the rest (i.e. 2^{nd}, 3^{rd} etc) singular values, the modulation of the neural response by one variable (e.g., target) is likely to be affected by the position of the other variable (e.g., hand), thus the responses are inseparable. To disambiguate between these two alternatives, neural responses were classified as separable if the first singular value was significantly larger (one-tailed t test, $p < 0.05$) compared to the first singular value calculated when conditions were randomized by permuting (Randomization test, 5000 permutations) the rows and the columns of the response matrix (Pesaran et al., 2006). In more detail, during the Randomization test the elements of the response matrix (i.e., the 9 mean firing rates, one per each condition) were permuted 5000 times and each rearranged matrix was subjected to SVD. The first singular values from all the rearranged matrices (N = 5000) formed a distribution that was used to test for statistical significance. If the first singular value of the original matrix was greater than 95% of the singular values in this distribution, then the neural responses were classified as separable. A mean value, computed from all 9 conditions, was subtracted from each of the 9 mean firing rates of the response matrix elements before performing the SVD.

Demixed principal component analysis

We applied a dimensionality reduction technique called demixed Principal Component Analysis (dPCA, Kobak et al., 2016), using freely available code: http://github.com/machenslab/dPCA. This method disentangled the variance of high-dimensional neural data into a sum of low-level dimensions that quantify the variance only relative to the behavioral parameters of the task. Accordingly, the decomposition performed by dPCA provides a comprehensive view of the structure in the neural data that is related to the experimentally controlled variables. In relation to the classic PCA, dPCA uses information about the task parameters (i.e., depth, direction and interaction) to calculate the percentage of variance accounted by each one of them. A condition-independent component that represents fluctuations of the population activity occurring during the task progress that are common in all conditions is calculated first and then the condition-dependent components that express the variance due to a specific task parameter are computed. For each brain area, a five-dimensional matrix of the firing rate was created: one dimension for the neurons in that brain area, one dimension for the three depth conditions, one dimension for the three directions, one dimension for the time, and one dimension for the trials. This five-dimensional matrix was used as input for the algorithm, but for calculating the demixed principal components, trial averages were used (i.e., a four-dimensional matrix), so the calculations were not influenced by the intrinsic trial-by trial variability of the neuronal firing. The algorithm was implemented using the following parameters: the first 20 components were calculated, the number of repetitions used for optimal lambda calculation was 10, the number of iterations for cross-validation was 100, and the number of shuffles used to compute the Monte Carlo chance distribution was set to 100, as detailed in Kobak et al. (2016).

Cell Reports, Volume *41*

Supplemental information

Anterior-posterior gradient in the integrated processing of forelimb movement direction and distance in macaque parietal cortex

Kostas Hadjidimitrakis, Marina De Vitis, Masoud Ghodrati, Matteo Filippini, and Patrizia Fattori

Supplemental Information

Hadjidimitrakis et al. Anterior-posterior gradient in the integrated processing of forelimb movement direction and distance in macaque parietal cortex

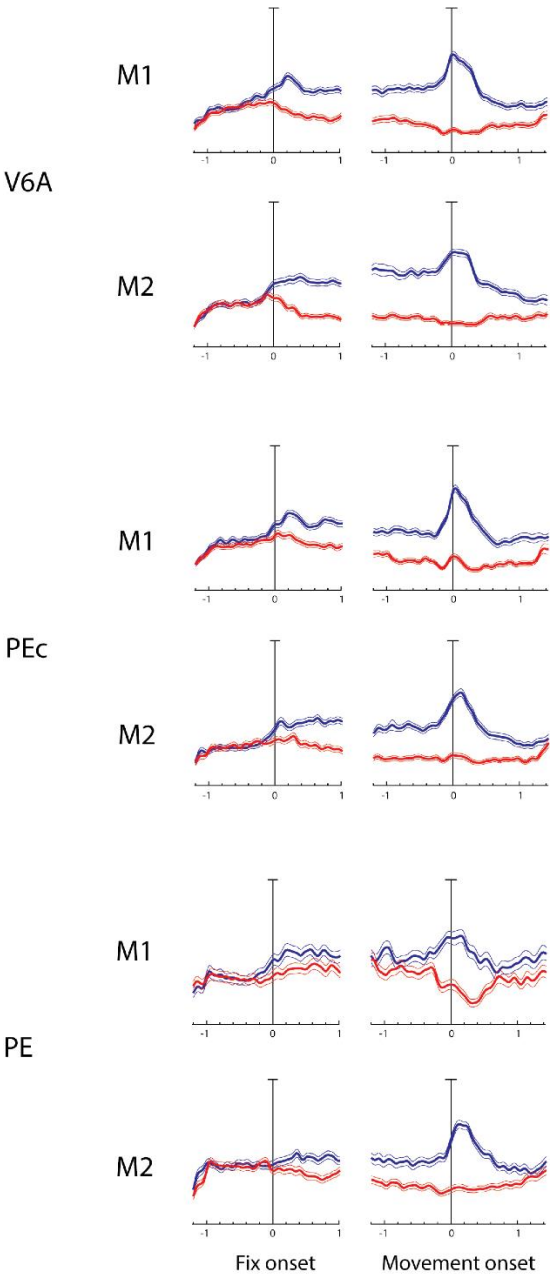

Supplementary Figure 1

Figure S1 (related to Figure 1). Population activity in individual monkeys. Average normalized spike density function (SDF) of recorded V6A, PEc and PE populations illustrated separately for each monkey. Each SDF was aligned twice at the fixation onset (left panels) and at the movement onset (right panels) and the average activity for the preferred (red curves) and non-preferred position (blue curves) are plotted. Thin black lines in SDFs represent the standard error of the mean. Vertical bars in all SDF plots: 100% of normalized activity.

Table S1 (related to Figure 2). Incidence of direction and depth effects in individual monkeys. Percentages of cells in Monkey 1/**Monkey 2** that showed tuning for depth only, direction only, and both factors in the different task epochs (two-way ANOVA, $p<0.01$).

	FIX			*PLAN*			*REACH*		
	depth only	dir only	both	depth only	dir only	both	depth only	dir only	both
V6A	21/**13**	17/**28**	16/**20**	22/**17**	11/**16**	12/**25**	27/**22**	15/**14**	18/**27**
PEc	16/**11**	22/**23**	10/**13**	16/**12**	14/**17**	8/15	25/**18**	13/**19**	15/**18**
PE	6/**9**	8/**12**	1/**3**	2/**9**	5/**6**	1/**2**	15/**16**	1/**8**	5/**8**

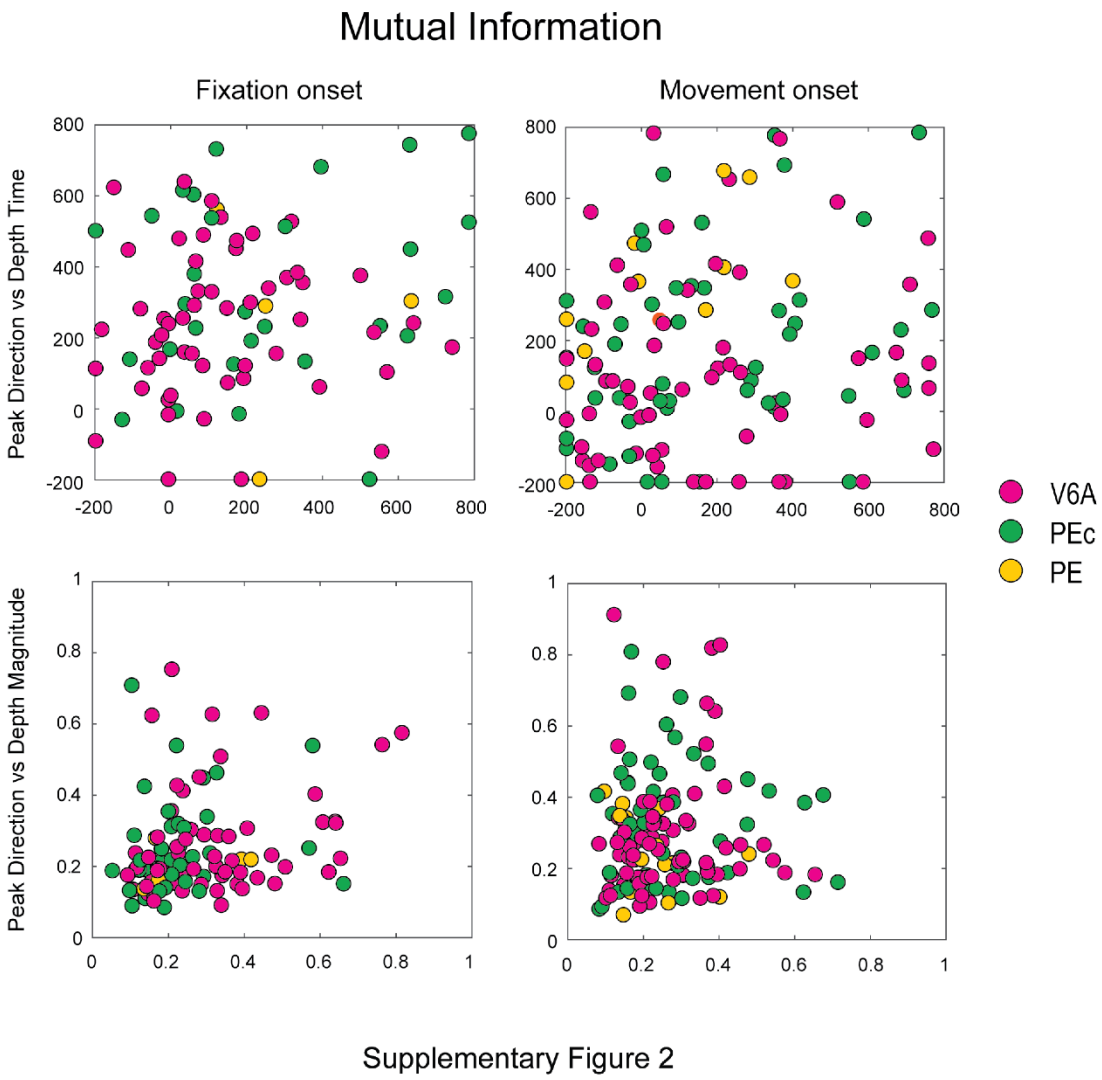

Supplementary Figure 2

Figure S2 (related to Figure 3). Mutual information in cells with combined direction and depth effects.

Timing (top panels) and magnitude (bottom panels) of directional and depth mutual information in neurons tuned by both depth and direction (two-way ANOVA, $p<0.05$) at fixation (left) and movement (right) onsets. Around fixation interval the directional MI led depth MI (left upper panel), whereas around hand movement this trend was preserved only in PE (right upper panel). In all areas the peak depth MI was significantly higher compared to directional MI around the movement period interval (Wilcoxon Rank sum test: $p<0.05$ for PE, $p<0.0001$ for PEc and V6A.

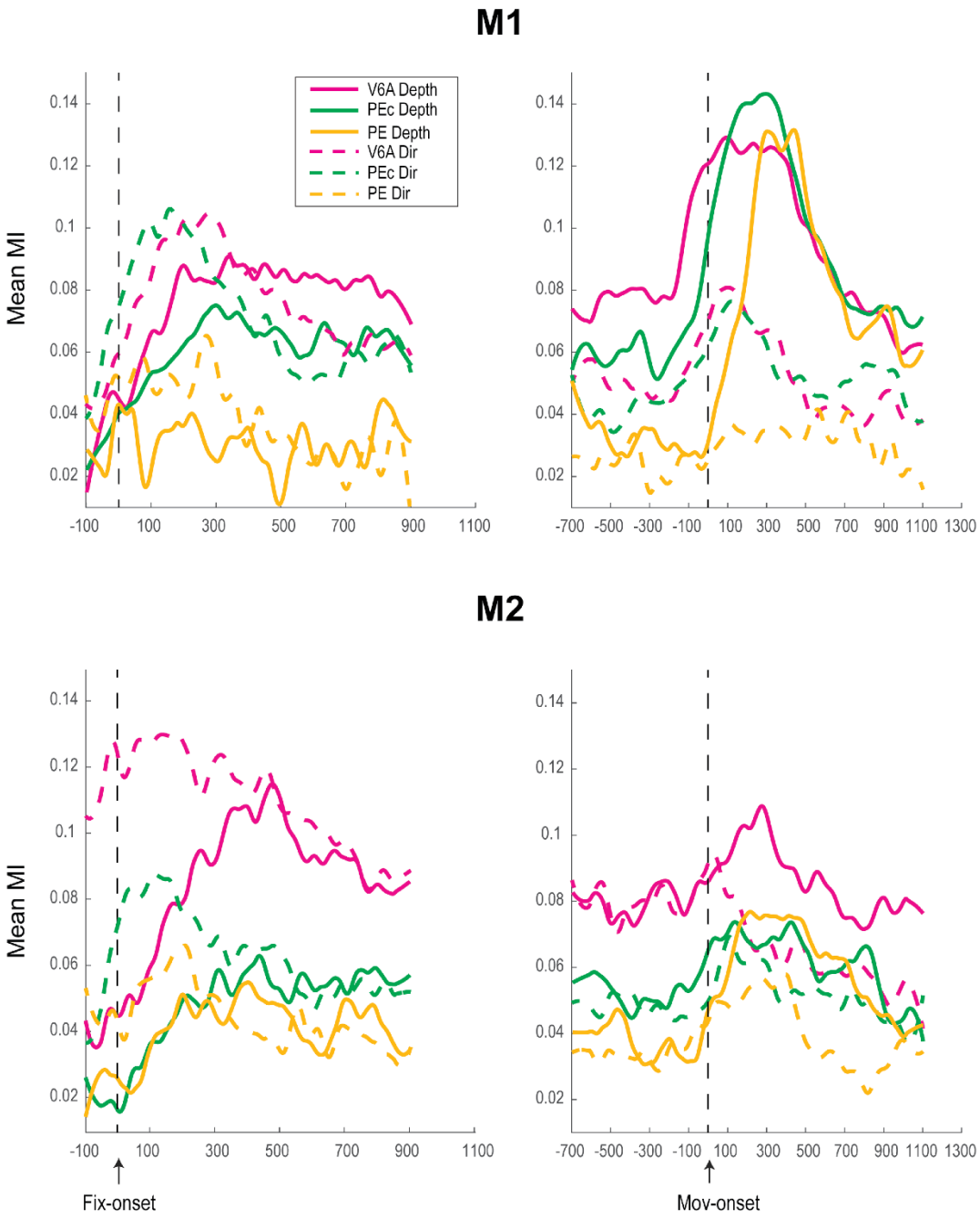

Supplementary figure S3

Figure S3 (related to Figure 3). Mean magnitude of depth (solid lines) and directional (dashed lines) mutual information in individual monkeys. Mean MI is aligned at fixation onset (left) and movement onset (right) across tuned cells (two-way ANOVA, $p<0.01$) in V6A, PEc and PE. Vertical dashed lines indicate the fixation (left) and movement (right) onsets.

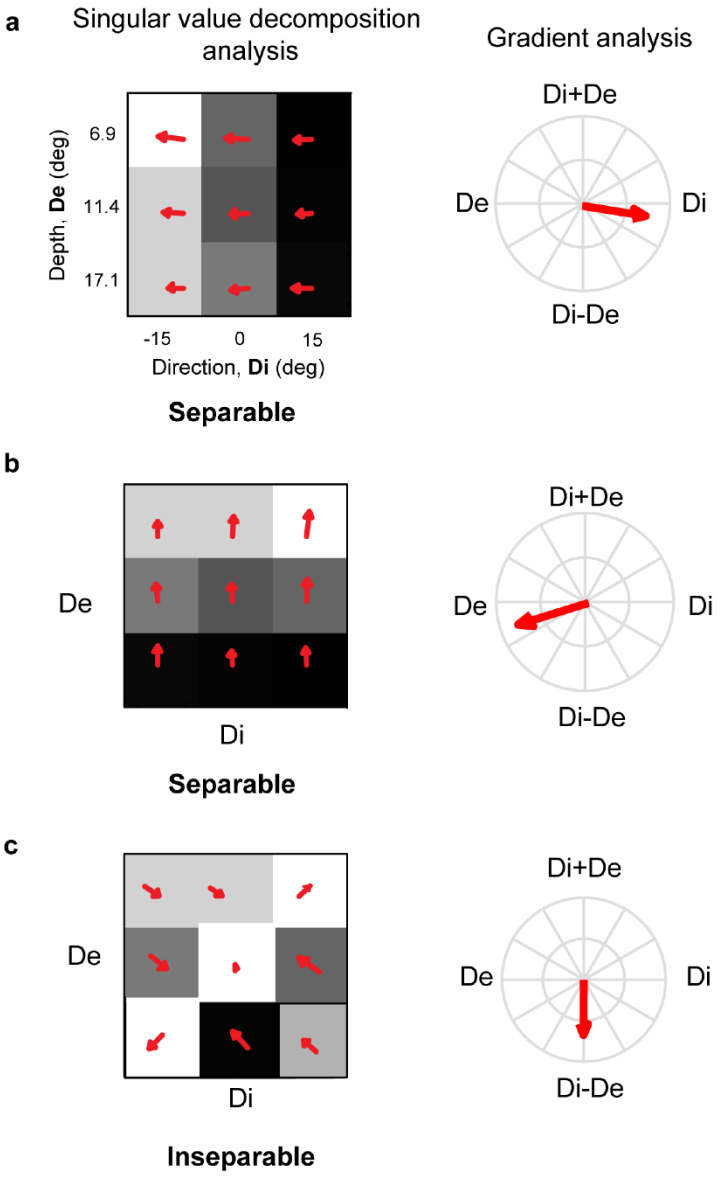

Supplementary Figure 4

Figure S4 (related to Figure 4). Gradient and separability analysis of modelled neural responses. A-C. Idealized neural responses. **A-B**: Weak modulation (gain field) of direction coding (Di) by depth (De) and vice versa. **C**: Vector relationship between Di and De. Left panels show idealized matrix responses for the Di and De pair of variables. White represents a high firing rate and black represents a low firing rate. Small red arrows show the gradient of each matrix response field. Right panels show the overall response field orientation calculated from the red gradient arrows. The response field orientation indicates the relative influence of each variable on the firing rate of the cell.

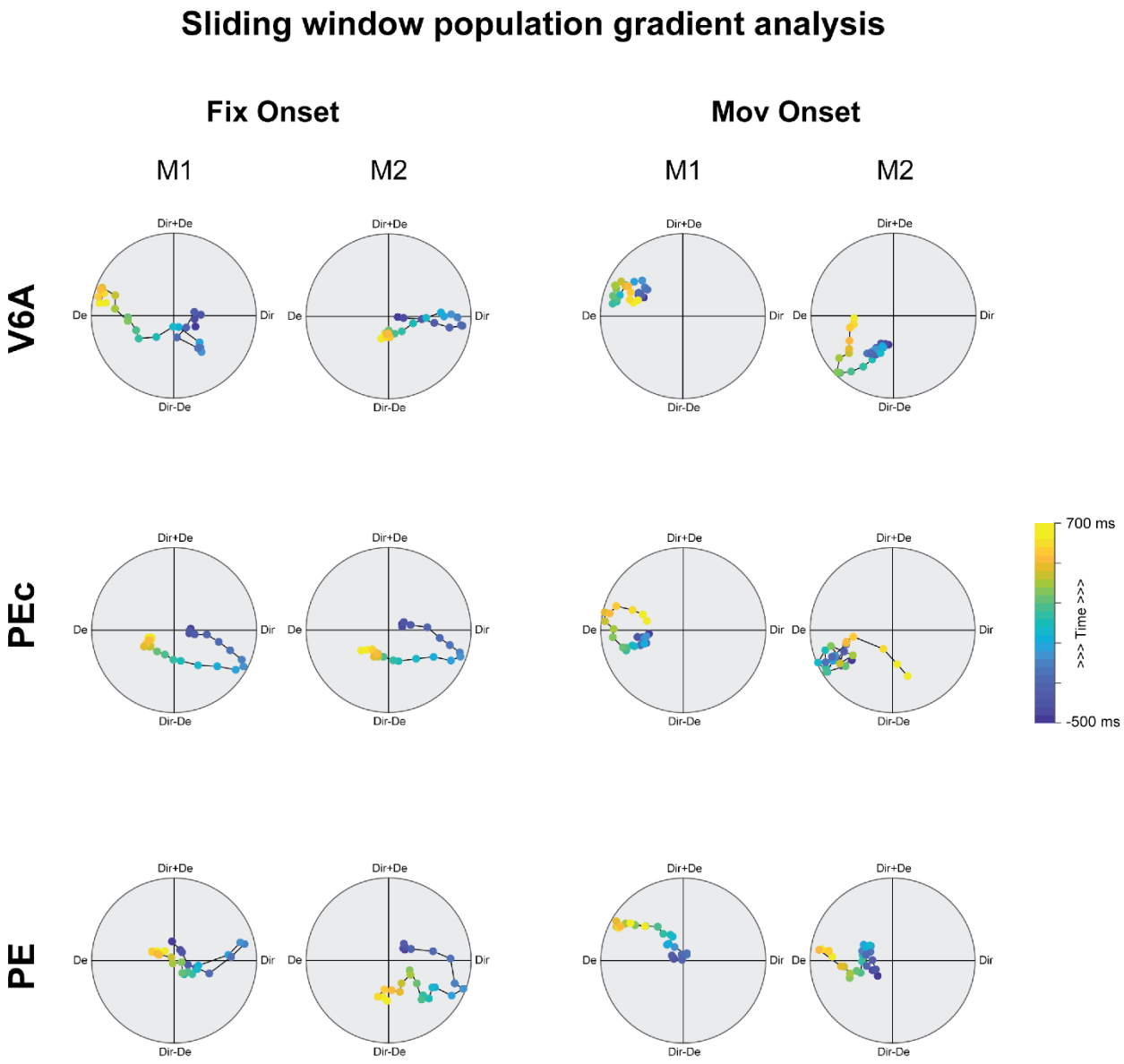

Supplementary figure S5

Figure S5 (related to Figure 4). Sliding window population gradient analysis in individual monkeys. Each data point corresponds to the angle of population's response field orientation, thus indicating which of the two variables has a stronger effect on activity at each time step. The distance from the center of the circle is proportional to the strength of tuning. Plots are aligned at fixation onset (two columns on the left) and movement onset (two columns on the right).

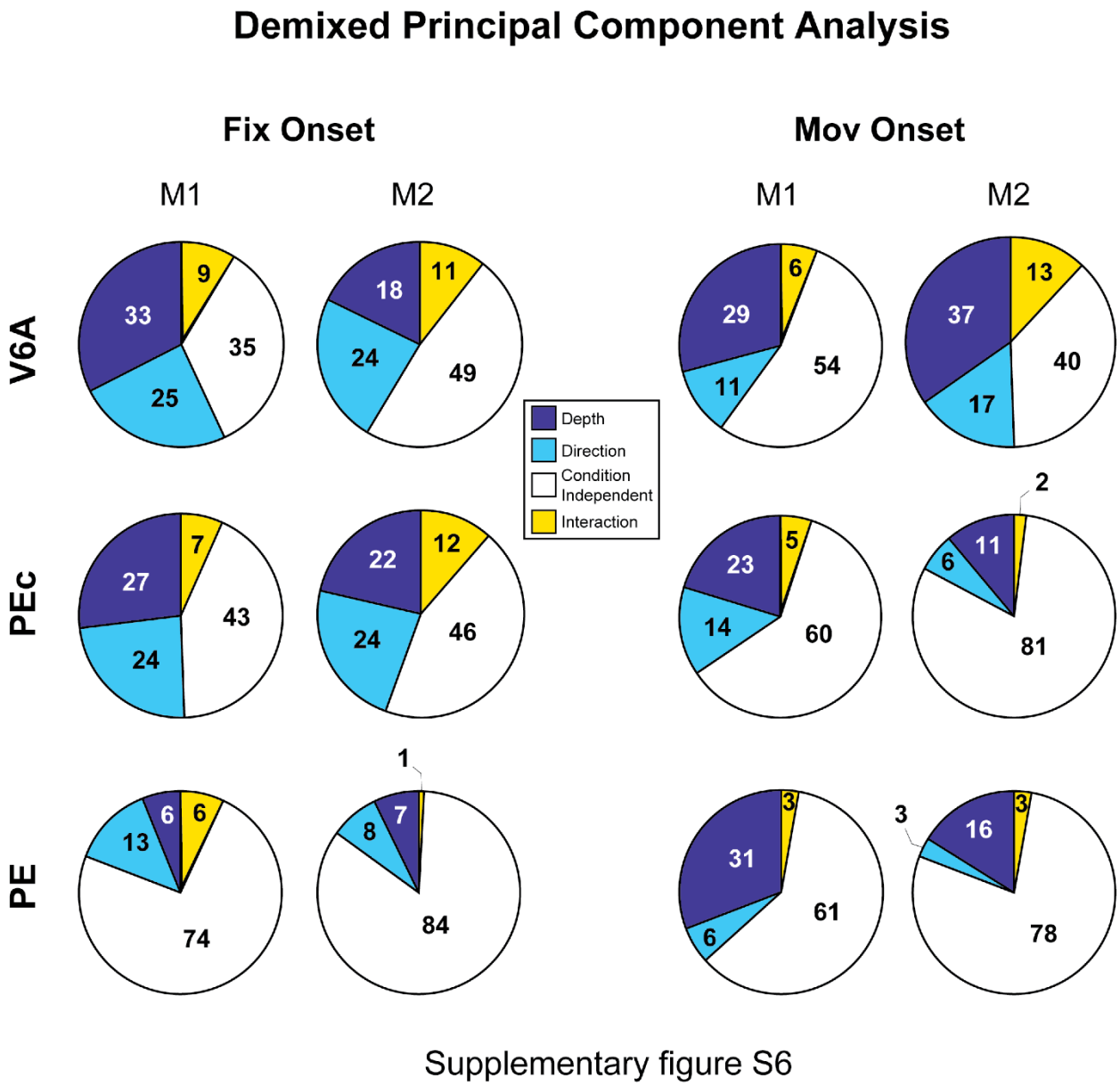

Supplementary figure S6

Figure S6 (related to Figure 5). Demixed Principal Component Analysis in individual monkeys. Pie charts showing the variance of the individual demixed principal components (depth, blue; direction, light blue; interaction, yellow; condition-independent, white) in each area, aligned at fixation onset (two columns on the left) and movement onset (two columns on the left right).